

1 **An observational study of the effects of aerosols on diurnal variation of heavy rainfall**
2 **and associated clouds over Beijing-Tianjin-Hebei**

3
4 Siyuan Zhou^{1,2,3}, Jing Yang^{1,2*}, Wei-Chyung Wang³, Chuanfeng Zhao⁴, Daoyi Gong^{1,2}, Peijun Shi^{1,2}

5
6 ¹ State Key Laboratory of Earth Surface Process and Resource Ecology, Beijing Normal University, China

7 ² Key Laboratory of Environmental Change and Natural Disaster, Faculty of Geographical Science, Beijing
8 Normal University, China

9 ³ Atmospheric Sciences Research Center, State University of New York, Albany, New York 12203, USA

10 ⁴ College of Global Change and Earth System Science, Beijing Normal University, China

11
12
13 Submitted to ACP

14 Oct 2018

15
16
17
18
19
20
21
22
23
24
25
26
27
28
29
30
31
32
33 *Correspondence to: Jing Yang, State Key Laboratory of Earth Surface Process and Resource Ecology/ Key
34 Laboratory of Environmental Change and Natural Disaster, Faculty of Geographical Science, Beijing Normal
35 University, 19#Xinjiekouwai Street, Haidian District, Beijing 100875, China. E-mail: yangjing@bnu.edu.cn

36 **Abstract:** Our previous study found that the observed rainfall diurnal variation over Beijing-Tianjin-Hebei
37 shows distinct signature of the effects of pollutants. Here we used the hourly rainfall data together with
38 satellite-based daily information of aerosols and clouds to further investigate changes in heavy rainfall and
39 clouds associated with aerosol changes. Because of the strong coupling effects, we also examined the
40 sensitivity of these changes to moisture (specific humidity) variations. For heavy rainfall, three distinguished
41 characteristics are identified: *earlier start time*, *earlier peak time*, and *longer duration*; and the signals are
42 robust using aerosol indicators based on both aerosol optical depth and cloud droplet number concentration.
43 In-depth analysis reveals that the first two characteristics occur in the presence of (absorbing) black carbon
44 aerosols and that the third is related to more (scattering) sulfate aerosols and sensitive to moisture abundance.
45 Cloud changes are also evident, showing increases in cloud fraction, cloud top pressure, the liquid/ice cloud
46 optical thickness and cloud water path, and decrease in ice cloud effective radius; and these changes are
47 insensitive to moisture. Finally, the mechanisms for heavy rainfall characteristics are discussed and
48 hypothesized.

49 **Key words: aerosol, heavy rainfall, diurnal variation, cloud, Beijing-Tianjin-Hebei, observational study**

50

51 **1. Introduction**

52 Aerosols modify the hydrologic cycle through direct radiative and indirect cloud adjustment effects (IPCC,
53 2013). The direct effect, through absorbing and scattering solar radiation, leads to heating in the atmosphere
54 (e.g. Jacobson 2001; Lau et al. 2006) and cooling on the surface (Lelieveld and Heintzenberg 1992; Guo et al.
55 2013; Yang et al., 2018), causing changes in atmospheric vertical static stability and subsequently modulation
56 of rainfall (e.g. Rosenfeld et al. 2008). On the other hand, water-soluble aerosols serving as cloud
57 condensation nuclei (CCN) affect the warm-rain and cold-rain processes through influencing the cloud droplet
58 size distributions, cloud top heights and other cloud properties (Jiang et al., 2002; Givati and Rosenfeld 2004;
59 Chen et al., 2011; Lim and Hong 2012; Tao et al., 2012). For Beijing-Tianjin-Hebei (BTH) the significant
60 increase in pollution in recent decades has raised issues concerning aerosol-radiation-cloud-precipitation
61 interactions. While the impact of aerosols on light rainfall or warm-rain processes is in general agreement
62 among studies for this region (e.g., Qian et al., 2009), the uncertainties of the effects on heavy convective
63 rainfall are still large (Guo et al., 2014; Wang et al., 2016).

64 The clouds that can generate heavy convective rainfall in BTH region usually contain warm clouds, cold
65 clouds and mixed-phase clouds (e.g. Guo et al., 2015). Because the aerosol-cloud interactions in different
66 types of clouds are distinct (Gryspeerdt et al., 2014b), aerosol indirect effect during heavy rainfall is more
67 complicated than its direct effect (Sassen et al., 1995; Sherwood, 2002; Jiang et al., 2008, Tao et al., 2012).
68 For warm clouds, by serving as CCN that nucleates more cloud droplets, aerosols can increase cloud albedo so
69 called albedo effect or Twomey effect (Twomey, 1977), lengthen the cloud lifetime so called lifetime effect

70 (Albrecht, 1989), and enhance thin cloud thermal emissivity so called thermal emissivity effect (Garrett and
71 Zhao, 2006). The above effects tend to increase the cloud microphysical stability and suppress warm-rain
72 processes (Albrecht 1989; Rosenfeld et al. 2014). For cold clouds and mixed-phase clouds, many studies
73 reported that the cloud liquid accumulated by aerosols is converted to ice hydrometeors above the freezing
74 level, which invigorates deep convective clouds and intensifies heavy precipitation so called invigoration
75 effect (Rosenfeld and Woodley, 2000; Rosenfeld et al., 2008; Lee et al. 2009; Guo et al. 2014). The Twomey
76 effect infers that aerosols serving as CCN that increase the cloud droplets could reduce cloud droplet size
77 within a constant liquid water path (Twomey, 1977). However, the opposite results of relationship between
78 aerosols and cloud droplet effective radius were reported in observations (Yuan et al., 2008; Panicker et al.,
79 2010; Jung et al., 2013; Harikishan et al., 2016; Qiu et al., 2017), which might be related with the moisture
80 supply near the cloud base (Yuan et al., 2008; Qiu et al., 2017). Besides, the influence of aerosols on ice
81 clouds also depends upon the amount of moisture supply (Jiang et al., 2008). Therefore, how the aerosols
82 modify the heavy convective rainfall and associated cloud changes does not reach a consensus, particularly if
83 considering the different moisture conditions.

84 Heavy convective rainfall over BTH region usually occurs within a few hours, thus studying on the
85 relationship between aerosols and rainfall diurnal variation could deepen our understanding of aerosol effects
86 on heavy rainfall. Several previous studies have found that aerosols are related to the changes of the rainfall
87 diurnal variation in other regions (Kim et al., 2010; Gryspeerd et al., 2014b; Fan et al., 2015; Guo et al., 2016;
88 Lee et al., 2016). However, the above studies do not address the change of cloud properties and its sensitivity
89 to different conditions of moisture supply. Although our recent work over BTH region (Zhou et al. 2018)
90 attempted to remove the meteorological effect including circulation and moisture and found that the peak of
91 heavy rainfall shifts earlier on the polluted condition, it only excluded the extreme moisture conditions and
92 focused on aerosol radiative effect on the rainfall diurnal variation. Therefore, this study aims to deepen the
93 previous study (Zhou et al., 2018) through investigating the following questions: (1) how do aerosols
94 (including absorbing aerosols and scattering aerosols) modify the behaviors of the heavy rainfall diurnal
95 variation (start time, peak time, duration and intensity)? And what is the role of moisture in them? (2) how do
96 aerosols influence the associated cloud properties with inclusion of moisture? To solve above questions, we
97 used aerosol optical depth (AOD) as a macro indicator of aerosol pollution and cloud droplet number
98 concentration (CDNC) as a micro indicator of CCN served by aerosols respectively to compare the
99 characteristics of heavy rainfall diurnal variation and cloud properties between clean and polluted conditions,
100 and applied aerosol index (AI) to distinguish the associated different effects of absorbing aerosols and
101 scattering aerosols. In addition, we used the specific humidity (SH) at 850 hPa as an indicator of moisture
102 supply condition to investigate the possible effects of moisture on the rainfall and clouds and compared them
103 with the effects of aerosols. The paper is organized as following: The data and methodology are introduced in
104 Sect. 2. Section 3 addresses the relationship between aerosol pollution and diurnal variation of heavy rainfall,
105 covering the distinct characteristics of heavy rainfall using AOD and CDNC; the different behaviors of heavy

106 rainfall diurnal variation along with different types of aerosols, and the comparison of heavy rainfall behaviors
107 influenced respectively by moisture and aerosols. Section 4 describes the concurrent changes of cloud
108 properties associated with aerosols and compares the possible influences of CDNC (CCN) and moisture on the
109 cloud properties. Section 5 gives the hypothesis about the mechanisms of aerosol effects on the heavy rainfall.
110 Conclusions and discussion will be given in Sect. 6.

111

112 **2. Approach**

113 **2.1 Data**

114 Four types of datasets from the year 2002 to 2012 (11 years) are used in this study, which include (1)
115 precipitation, (2) aerosols, (3) clouds, and (4) other meteorological fields.

116 **2.1.1 Precipitation**

117 To study the diurnal variation of heavy rainfall, the gauge-based hourly precipitation datasets are used, which
118 were obtained from the National Meteorological Information Center (NMIC) of the China Meteorological
119 Administration (CMA) (Yu et al., 2007) at 2420 stations in China from 1951 to 2012. The quality control
120 made by CMA/NMIC includes the check for extreme values (the value exceeding the monthly maximum in
121 daily precipitation was rejected), the internal consistency check (wiping off the erroneous records caused by
122 incorrect units, reading, or coding) and spatial consistency check (comparing the time series of hourly
123 precipitation with nearby stations) [Shen et al., 2010]. Here we chose 176 stations in the plain area of BTH
124 region that are below the topography of 100 meter above sea level as shown in Fig.1, because we purposely
125 removed the probable orographic influence on the rainfall diurnal variation, which is consistent with our
126 previous work (Zhou et al., 2018). The record analyzed here is the period of 2002 to 2012. We selected heavy
127 rainfall days when the hourly precipitation amount is more than 8.0 mm/hour (defined by *Atmospheric*
128 *Sciences Thesaurus, 1994*). Here “a day” is counted from 8 LST to 8 LST next day (0 UTC to 24 UTC).

129 **2.1.2 Aerosols**

130 In this study, we used two satellite data and one reanalysis data to investigate the aerosol optical amount and
131 distinguish the different aerosol types.

132 AOD is a proxy for the optical amount of aerosol particles in a column of the atmosphere and serves as the
133 macro indicator for the division of aerosol pollution condition in this study, which was obtained from MODIS
134 (Moderate Resolution Imaging Spectroradiometer) Collection 6 L3 aerosol product with the horizontal
135 resolution of $1^{\circ} \times 1^{\circ}$ onboard the Terra satellite (Tao et al., 2015). The quality assurance of marginal or higher
136 confidence is used in this study. The reported uncertainty in MODIS AOD data is on the order of (-0.02-10%),
137 (+0.04+10%) (Levy et al., 2013). The Terra satellite overpass time at the equator is around 10:30 local solar
138 time (LST) in the daytime, and the satellite data is almost missing when it is rainy during the overpass time.

139 As shown in Fig.3, the occurrence of selected heavy rainfall events in this study is mainly later than the
140 satellite overpass time. Therefore, the AOD used here represents the situation of the air quality in advance of
141 heavy rainfall appearance. Many studies have indicated the value of AOD is influenced by moisture condition,
142 which is aerosol humidification effect (Twohy et al., 2009; Altaratz et al., 2013). Hence, we comprehensively
143 analyzed the moisture effect on the rainfall and tried to remove the moisture effect from the relationship
144 between aerosols and rainfall/clouds.

145 The ultraviolet AI from Ozone Monitoring Instrument (OMI) on board the Aura satellite which was
146 launched in July 2004, is used for detecting the different types of aerosols in this study. The OMI ultraviolet
147 AI is a method of detecting absorbing aerosols from satellite measurements in the near-ultraviolet wavelength
148 region (Torres et al., 1998). The positive values of ultraviolet AI are attributed to the absorbing aerosols such
149 as smoke and dust while the negative values of AI stand for the non-absorbing aerosols (scattering aerosols)
150 such as sulfate and sea salt (Tariq and Ali, 2015). The near-zero values of AI occur when clouds and Rayleigh
151 scattering dominate (Hammer et al., 2018). Considering the near-zero values have more uncertainties, we only
152 compare the extreme circumstances of absorbing aerosols and scattering aerosols in this study. The horizontal
153 resolution of AI data is $1^{\circ}\times 1^{\circ}$ and it covers the period of 2005 to 2012.

154 MACC-II (Monitoring Atmospheric Composition and Climate Interim Implementation) reanalysis product
155 produced by ECMWF (the European Centre for Medium-Range Weather Forecasts), provided the AOD
156 datasets for different kinds of aerosols (BC, sulfate, organic matter, mineral dust and sea salt). MACC-II
157 reanalysis products are observationally-based within a model framework, which can offer a more complete
158 temporal and spatial coverage than observation and reduce the shortcomings of simulation that fail in
159 simulating the complexity of real aerosol distributions (Benedetti *et al.*, 2009). The horizontal resolution of
160 MACC-II is also $1^{\circ}\times 1^{\circ}$ with the time interval of six-hour, and the results in the analysis of heavy rainfall show
161 consistent based on the daily mean values which is shown in the figures and morning values that before the
162 occurrence of heavy rainfall. MACC-II data covers the period of 2003 to 2012.

163 **2.1.3 Clouds**

164 Daily cloud variables, including cloud fraction (CF), cloud top pressure (CTP), cloud optical thickness (COT,
165 liquid and ice), cloud water path (CWP, liquid and ice) and cloud effective radius (CER, liquid and ice), were
166 obtained from MODIS Collection 6 L3 cloud product onboard the Terra satellite. The MODIS cloud product
167 combines infrared emission and solar reflectance techniques to determine both physical and radiative cloud
168 properties (Platnick et al., 2017). The validation of cloud top properties in this product has been conducted
169 through comparisons with CALIOP (Cloud-Aerosol Lidar with Orthogonal Polarization) data and other lidar
170 observations (Holz et al., 2008; Menzel et al., 2008), and the validation and quality control of cloud optical
171 products is performed primarily using in situ measurements obtained during field campaigns as well as the
172 MODIS Airborne Simulator instrument (<https://modis-atmos.gsfc.nasa.gov/products/cloud>). Consistent with
173 AOD, the measure of above cloud variables is before the occurrence of heavy rainfall.

174 In addition to the variables in MODIS cloud product, we also calculated CDNC using the liquid COT and
 175 CER in this product. CDNC is retrieved as the proxy for CCN and also the micro indicator for separating
 176 different aerosol conditions in this study. Currently, most derivations of CDNC assume that the clouds are
 177 adiabatic and horizontally homogeneous; CDNC is constant throughout the cloud's vertical extent, and cloud
 178 liquid water content varies linearly with altitude adiabatically (Min et al., 2012; Bennartz and Rausch, 2017).
 179 According to Boers et al. (2006) and Bennartz (2007), we calculated CDNC (unit: cm^{-3}) through:

$$180 \quad \text{CDNC} = \frac{C_w^{1/2}}{k} \frac{10^{1/2}}{4\pi\rho_w^{1/2}} \frac{\tau^{1/2}}{R_e^{5/2}} \quad (1)$$

181 Where C_w is the moist adiabatic condensate coefficient, and its value depends slightly on the temperature
 182 of the cloud layer, ranging from 1 to $2.5 \times 10^{-3} \text{ gm}^{-4}$ for a temperature between 0 °C and 40 °C (Brenguier,
 183 1991). In this study, we calculated the C_w through the function of the temperature (see Fig.1 in Zhu et al.,
 184 2018) at a given pressure that is 850 hPa. And we have tested the sensitivity of CDNC to the amount of C_w
 185 and found it almost keeps the same when the C_w changes from 1 to $2.5 \times 10^{-3} \text{ gm}^{-4}$. The coefficient k is the
 186 ratio between the volume mean radius and the effective radius, and varies between 0.5 and 1 (Brenguier et al.,
 187 2000). Here we used $k = 1$ for that we cannot get the accurate value of k and the value of k does not influence
 188 the rank of CDNC for the division of aerosol condition in this study. ρ_w is cloud water density. τ and Re are
 189 the liquid COT and CER obtained from MODIS Collection 6 L3 cloud product with resolution of $1^\circ \times 1^\circ$. To
 190 reduce the uncertainty of CDNC retrieval caused by the heterogeneity effect from thin clouds (Nakajima and
 191 King, 1990; Quaas et al., 2008; Grandey and Stier, 2010; Grosvenor et al., 2018), we selected the CF more
 192 than 80%, the liquid COT more than 4 and the liquid CER more than $4 \mu\text{m}$ when calculating the CDNC
 193 (Quaas et al., 2008).

194 **2.1.4 Other meteorological data**

195 In this study, wind, temperature, pressure and SH data, were obtained from the ERA-Interim reanalysis
 196 datasets with $1^\circ \times 1^\circ$ horizontal resolution and 37 vertical levels at six-hour intervals. The daily mean values of
 197 these variables are used in the study, and we also verified the results based on the morning values that before
 198 the occurrence of heavy rainfall. ERA-Interim is a global atmospheric reanalysis produced by ECMWF,
 199 which covers the period from 1979 to near-real time (Dee et al., 2011). The SH, which stands for the water
 200 vapor content, serves as the indicator of moisture supply condition in this study.

201

202 **2.2 Methodology**

203 We used both station data of gauge-based precipitation and gridded data including aerosols, clouds and other
 204 meteorological variables. Gridded datasets in this study were downloaded with the horizontal resolution of
 205 $1^\circ \times 1^\circ$, which are consistent with the resolution of MODIS L3 products. To unify the datasets, we interpolated
 206 all the gridded datasets onto the selected 176 rainfall stations using the average value in a $1^\circ \times 1^\circ$ grid as the

207 background condition of each rainfall station, i.e., the stations in the same $1^{\circ}\times 1^{\circ}$ grid have the same aerosol,
208 cloud and meteorological conditions.

209 **2.2.1 Selection of sub-season and circulation**

210 Consistent with our previous work, we focused on the early summer period (1 June to 20 July) which is before
211 the large-scale rainy season start, in order to remove the large-scale circulation influence and identify the effect
212 of aerosols on local convective precipitation because BTH rainfall during this period is mostly convective
213 rainfall (Yu et al., 2007) with heavy pollution (Zhou et al., 2018). And to unify the background atmospheric
214 circulation, we only selected the rainfall days with southwesterly flow, which is the dominant circulation
215 accounting for 40% of total circulation patterns over the BTH region during early summer (Zhou et al., 2018).

216 **2.2.2 Classification of clean/polluted cases and moisture conditions**

217 With the circulation of southwesterly, we used two indicators to distinguish the clean and polluted conditions
218 from macro and micro perspectives, which are AOD and CDNC. The 25th and 75th percentiles of AOD/CDNC
219 of the whole rainfall days are used as the thresholds of clean and polluted conditions, and the values are
220 shown in Tab.1. There are 514 cases of heavy rainfall on the polluted days and 406 cases of that on the clean
221 days when using AOD, and 630/716 cases on the polluted/clean condition when using CDNC (Fig. 3).

222 The absorbing aerosols are detected using the positive values of AI that is named as absorbing aerosol index
223 (AAI) here, and we can retrieve the scattering aerosol index (SAI) using the negative values of AI. AAI and
224 SAI are also divided into two groups using the threshold of 25th/75th percentile as shown in Tab.1. We used
225 AAI/SAI more than 75th percentile as the extreme circumstances of absorbing/scattering aerosols to compare
226 their impacts on the heavy rainfall. The sample numbers are 375 and 550 respectively for the extreme AAI
227 and SAI cases. Using the same method, we chose cases with more BC/sulfate when the AOD of BC/sulfate is
228 larger than the 75th percentile of itself in all rainy days, and cases with less BC/sulfate when that is less than
229 the 25th percentile of itself in the same situation. Accordingly, we selected 459 heavy rainfall cases with more
230 BC and 274 cases with less BC. Similarly, 361 cases with more sulfate and 419 cases with less sulfate were
231 selected (Fig. 6).

232 The SH at 850 hPa is used as the indicator of moisture supply under the cloud base. We chose wet cases
233 when the SH on that day is larger than 75th percentile of the whole rainy days, and chose dry cases when SH
234 on that day is less than the 25th percentile of the whole rainy days (the thresholds are shown in Tab. 1).

235 **2.2.3 Statistical analysis**

236 We adopted the probability distribution function (PDF) to compare the features of heavy rainfall and cloud
237 variables on different conditions of aerosols, through which we can understand the changes of rainfall/cloud
238 properties more comprehensively. The numbers of bins we selected in the study have been all tested for better
239 representing the PDF distribution. Student's t-test is used to examine the significance level of differences

240 between the different groups of aerosol conditions. The differences between any two groups that have passed
241 95% statistical confidence level are considered significant. And two variables are considered correlated when
242 the correlation coefficient is more than 0.5 or less than -0.5.

243

244 **3. Changes of heavy rainfall**

245 In this study, we used two indicators (AOD and CDNC) to identify the aerosol pollution. AOD is usually
246 used as the macro indicator of aerosol pollution, which represents the optical amount of aerosol particles.
247 However, AOD is not a proper proxy for CCN (Shinozuka et al., 2015), but the property of aerosols serving as
248 CCN should be considered because aerosol-cloud interaction plays an indispensable role on changing rainfall
249 diurnal variation. Therefore, here we applied the retrieved CDNC as the indicator of CCN (Zeng et al., 2014;
250 Zhu et al., 2018).

251 We first investigated the value distribution of AOD and CDNC over the BTH region. Figure 2a&b shows
252 the PDFs of AOD and CDNC on the non-rainfall days, rainfall days and heavy rainfall days respectively. The
253 spectral distributions of AOD on different conditions are quite similar that the ranges are all between 0-5 and
254 the peaks occur at around 1.2 (Fig. 2a). In contrast, CDNC shows different ranges between different
255 conditions, that it ranges from around 20 cm^{-3} to 500 cm^{-3} on the rainfall days and non-rainfall days while
256 from around 30 cm^{-3} to 420 cm^{-3} on the heavy rainfall days. Besides, the proportion of low CDNC is quite
257 high on the non-rainfall days (Fig. 2b). The averaged CDNCs on the non-rainfall days, rainfall days and heavy
258 rainfall days are 54.70, 72.92, and 68.66 cm^{-3} respectively. According to the above results, the range of AOD
259 remains similar on the heavy rainfall days while the range of CDNC is shortened, probably because the cloud
260 droplets become larger before heavy rainfall so that the number concentration becomes less. Therefore, to
261 obtain comparable samples, we use percentile method to select respective clean and polluted cases based on
262 above two indicators and compare the characteristics of heavy rainfall. Hence the heavier pollution means
263 larger optical amount of aerosols measured by AOD, and more aerosols that could serve as CCN measured by
264 CDNC.

265 **3.1 Characteristics**

266 Our previous study (Zhou et al. 2018) has reported the distinct peak shifts of rainfall diurnal variation between
267 clean and polluted days using the indicator of AOD over the BTH region during early summer. Similar with
268 our previous study, the PDF of the heavy rainfall peak time shows that the maximum of rainfall peak is about
269 two hours earlier on the polluted days (20:00 LST) than that on the clean days (22:00 LST) (Fig. 3a). To
270 comprehensively recognize the changes of rainfall diurnal variation associated with air qualities, here we
271 examined the PDF of the start time, the duration and the intensity besides the peak time of heavy rainfall.

272 As shown in Fig. 3a, the start time of heavy rainfall exhibits a significant advance on the polluted days. The
273 secondary peak on the early morning is ignored here because the early-morning rainfall is usually associated

274 with the mountain winds (Wolyn et al., 1994; Li et al., 2016) and the nighttime low-level jet (Higgins et al., 1997;
275 Liu et al., 2012) that is beyond the scope of this study. The time for the maximum frequency of heavy rainfall
276 initiation is around 6 hours earlier on the polluted days, shifting from around 0:00 LST on the clean days to
277 the 18:00 LST (Fig. 3a). Regarding the rainfall durations, the average persistence of heavy rainfall on polluted
278 days is 0.8 hours longer than that on clean days (Tab. 2). According to the PDF shown as in Fig. 3a, the
279 occurrence of short-term precipitation (≤ 6 hours, Yuan et al., 2010) decreases while that of long-term
280 precipitation (> 6 hours, Yuan et al., 2010) increases. The intensity of hourly rainfall exhibits a non-significant
281 increase on the polluted days.

282 The distinct behaviors of heavy rainfall diurnal variation between clean and polluted days have been well
283 demonstrated using the indicator of AOD. Using CDNC as the indicator of CCN, the above-mentioned results
284 are also significant, as shown in Fig. 3b. The start time and peak time of heavy rainfall on the polluted
285 condition also show significant advances compared with that on the clean condition, with the average
286 advances of 1.4 hours and 3.0 hours respectively (Tab. 2). The duration of heavy rainfall on the polluted
287 condition is also prolonged, which is 2.2 hours longer in average (Tab. 2). Similar with the results based on
288 AOD, the difference of rainfall intensity between clean and polluted conditions using CDNC does not pass the
289 95% statistical confidence level as well.

290 Hence, the results using either AOD or CDNC show that the start and peak time of heavy rainfall occur
291 earlier and the duration becomes longer under pollution, although there are some quantitative differences
292 between the two indicators. We found the AOD and CDNC only have a non-significant positive correlation,
293 which denotes that the selected cases could be different between using AOD and CDNC. The cases of heavy
294 rainfall using CDNC seem more extreme, because the rainfall behaviors exhibit more evident changes using
295 CDNC than using AOD. The result differences between the two indicators might be attributed to the
296 non-linear relationship between CCN and aerosol pollution (e.g., Jiang et al., 2016), the misdetection of AOD
297 when the humidity is high (Boucher and Quaas, 2012), the calculation uncertainty of CDNC, and the sampling
298 differences between AOD and CDNC. Since the two indicators represent aerosols from the different
299 perspectives, we cannot identify which one is more reliable. Because the change of rainfall intensity is not
300 significant using either AOD or CDNC, the following analysis only focuses on studying the start time, peak
301 time and duration of heavy rainfall along with aerosol pollution.

302 **3.2 Sensitivities to aerosol types**

303 Using the indicator of AI, we further investigated the distinct behaviors of heavy rainfall diurnal variation
304 related to absorbing aerosols and scattering aerosols respectively. The PDF of start time, peak time and
305 duration of heavy rainfall under the extreme circumstances of absorbing aerosols and scattering aerosols are
306 compared in Fig. 4. Here, we briefly named the days with extreme large amount of absorbing aerosols as
307 absorbing aerosol days and with more scattering aerosols as scattering aerosol days. The start time of heavy
308 rainfall on absorbing aerosol days shows a significant earlier compared with that on scattering aerosol days

309 (Fig. 4a), with 0.7 hours advance in average (Tab. 3). Similarly, the rainfall peak time also shows earlier on
310 absorbing aerosol days (Fig. 4b), with an average advance of 1.6 hours (Tab. 3). The rainfall duration on
311 scattering aerosol days shows longer than that on absorbing aerosol days, which are 6.0 hours and 5.0 hours
312 respectively in average (Tab. 3). All the above-mentioned differences between the two groups have passed 95%
313 statistical confidence level. The results indicate that the absorbing aerosols and scattering aerosols may have
314 different or inverse effects on the heavy rainfall that absorbing aerosols may generate the heavy rainfall in
315 advance while the scattering aerosols may delay and prolong the heavy rainfall.

316 To further verify the different behaviors of heavy rainfall diurnal variation associated with two different
317 types of aerosols, we purposely re-examine the above-mentioned phenomena using BC/sulfate that can
318 represent typical absorbing/scattering aerosols over the BTH region. BC has its maximum center over BTH
319 region (Fig. 5a) and our previous study has indicated that the radiative effect of BC low-level warming may
320 facilitate the convective rainfall generation (Zhou et al., 2018). The percentage of sulfate is also large over the
321 BTH region (Fig. 5b) and the sulfate is one of the most effective CCN that influences the precipitation in this
322 region (Gunthe et al., 2011). Accordingly, we selected the cases with different amounts of BC and sulfate
323 AOD to compare their roles on the diurnal variation of heavy rainfall. The methods have been described in
324 Sect. 2.2.2. The PDF of the start time, peak time and duration of heavy rainfall in the cases with more/less
325 amount of BC are shown in Fig. 6a, respectively. The most striking result is that the maximum frequency of
326 rainfall start time in the more BC cases evidently shifts earlier (Fig. 6a). Meanwhile, the mean peak time in
327 the more BC cases shows 1.1 hour earlier than that in the less BC cases (Tab. 3). And the duration of heavy
328 rainfall is slightly shortened by the averaged 0.2 hours in the more BC cases. The features in more BC cases
329 are consistent with the above results of absorbing aerosols. In contrast, when the sulfate has higher amount,
330 the mean start time of rainfall is delayed by 0.5 hours, while the duration shows a significant increase by 1.5
331 hours in average (Tab. 3). The behaviors in the more sulfate cases also exhibit similar with the above results
332 of scattering aerosols, except for the peak time that shows later in the scattering aerosol cases but a little
333 earlier in the more sulfate cases (Tab. 3).

334 **3.3 Influence of moisture**

335 Moisture supply is an indispensable factor for the precipitation formation, and it also has an important impact
336 on AOD (Boucher and Quaas, 2012). Since the southwesterly circulation can not only transport pollutants but
337 also plenty of moisture to the BTH region (Wu et al., 2017), more pollution usually corresponds to more
338 moisture for the BTH region (Sun et al., 2015) so that it is hard to completely remove the moisture effect on
339 the above results in the pure observational study. Here we attempt to recognize the moisture effect on the
340 heavy rainfall to further understand the above aerosol-associated changes. Because the moisture supply for
341 BTH is mainly transported via low-level southwesterly circulation, we purposely used the SH at 850 hPa as
342 the indicator of moisture condition.

343 Using the similar percentile method with polluted/clean days, we compared the heavy rainfall

344 characteristics in the more humid (more than 75th percentile) and the less humid (less than 25th percentile)
345 environments regardless of the aerosol condition, as shown in Fig. 7a. The results show that the start time of
346 heavy rainfall is delayed by 0.9 hours, the peak time is 0.6 hours earlier and the duration is prolonged by 2.0
347 hours in average in the more humid environment, which is similar with the results of the more sulfate cases.
348 Besides, the same results are obtained using different moisture indicator, e.g. the 850 hPa absolute humidity.
349 These results indicate the advance of heavy rainfall start time on the polluted days is not caused by more
350 moisture supply, while the longer duration and earlier peak in the more sulfate cases might be related to the
351 increased moisture supply. To further identify the role of sulfate, we tested the sensitivities of the results
352 associated with sulfate when limiting the moisture condition. In the dry and intermediate cases (SH less than
353 25th percentile and SH between 25th -75th percentiles), the heavy rainfall still shows later start time, earlier
354 peak and significant longer duration with the increase of sulfate, while the change of peak time is not
355 significant in the dry cases and that of start time is not significant in the intermediate cases; in the high
356 moisture cases (SH more than 75th percentile), it shows earlier peak and shorter duration in the more sulfate
357 cases while the change of start time is not significant. Therefore, we suppose that the impact of sulfate
358 aerosols on the heavy rainfall is sensitive to moisture, and notably the sulfate could contribute to the longer
359 duration in the polluted cases when it is relatively dry.

360 We also investigate the distributions of moisture and rainfall behaviors in the clean and polluted cases
361 respectively using AOD and CDNC (Fig. 7 b&c). The results show that the relationship between moisture and
362 rainfall start time/peak time/duration is not linear. Using either AOD or CDNC, the distribution of SH exhibits
363 a slight increase in the polluted cases, indicating that the polluted cases have the more moisture than the clean
364 cases which is particularly well shown using AOD. However, when fixing the moisture at a certain range
365 especially at the relative dry condition, we can detect the similar phenomena of earlier start/peak time and
366 longer duration in the polluted cases. For example, when the amount of 850 hPa SH is between 8-12 g/kg, the
367 start & peak time in the polluted cases show significant earlier and the duration exhibits slightly increased
368 compared with that in the clean cases using either AOD or CDNC. To further clarify the characteristics of
369 heavy rainfall associated with pollution, we removed the samples with high SH (SH more than 75th percentile)
370 and found that the results in section 3.1 remain the same, that when SH is less than 12.95 g/kg (75th percentile),
371 the start/peak time of heavy rainfall is also in advance and the duration is still prolonged with the increase of
372 AOD/CDNC (Fig. 8).

373 The above results indicate that the advance of heavy rainfall start in the polluted cases is independent of
374 moisture, while the advance of peak time and longer duration might be related to the moisture effect. For the
375 peak time of heavy rainfall, although the results of BC, sulfate and moisture show consistent advance, we
376 suppose the role of BC (absorbing aerosols) might be dominant compared with that of sulfate or moisture
377 because the change of peak time in the former analysis is much larger (Tab. 3). Both sulfate and moisture may
378 contribute to the longer duration of heavy rainfall (Fig. 6b&7a), but the role of sulfate seems sensitive to the
379 moisture condition, that the duration in the more sulfate cases is longer when the moisture condition is

380 relatively dry while becomes shorter when it is extremely wet. Because we cannot completely separate the
381 sulfate and moisture, we are not quite clear about their individual roles at present. Overall, under the condition
382 of removing the extremely high moisture cases, the earlier start/peak time and longer duration of heavy
383 rainfall associated with aerosol pollution are significant and irrespective of moisture.

384

385 **4. Changes of clouds**

386 To understand the cloud effect of aerosols during heavy rainfall diurnal variation, we need to recognize the
387 associated cloud characteristics on the clean and polluted conditions. The cloud properties we used were
388 obtained from satellite product that were measured at the same time with aerosols before the occurrence of
389 heavy rainfall. The differences of cloud features were examined in both macroscopic (including CF, CTP,
390 COT and CWP) and microscopic properties (including CER) between the clean and polluted conditions based
391 on AOD and CDNC respectively.

392 **4.1 Characteristics**

393 Using AOD as the macro aerosol indicator, as shown in Fig. 9, the PDF distribution of CF shows that the CF
394 on the polluted condition is evidently larger than that on the clean condition. The average CF is 62.8% on the
395 clean condition, and 89.3% on the polluted condition (Tab. 4), which is increased by 26.1%. The average CTP
396 on the polluted condition is 487.3 hPa, which is larger than 442.3 hPa on the clean condition, indicating that
397 the cloud top height is lower on the polluted days. The COT, CWP and CER were further analyzed for the
398 liquid and ice portions of clouds as shown in Fig. 9. Both liquid and ice COT on the polluted condition exhibit
399 significant increases compared with that on the clean condition. The mean amount of liquid COT is increased
400 by 3.1 and ice COT increases by 6.2 (Tab. 4). Similar with COT, the amounts of liquid and ice CWP also
401 increase under pollution, which increase by 33.6 g/m² and 88.2 g/m² respectively. In addition, the liquid CER
402 is increased by 0.8 μm and the ice CER is decreased by 2.8 μm on the polluted days. The differences of above
403 cloud properties between clean and polluted cases have all passed the 95% statistical confidence level.

404 Using CDNC as the micro aerosol indicator, the above-mentioned changes of cloud properties are
405 consistent with that using AOD, except for liquid CER (Fig. 9). Since the calculation method of CDNC is not
406 independent on the liquid COT and liquid CER, we would not directly compare the results of liquid COT and
407 CER based on CDNC with those based on AOD here. But according to other variables that are independent of
408 the CDNC calculation, we found the cases with more CDNC are accompanied with the increase of CTP, ice
409 COT and liquid & ice CWP, which increase by 32.8 hPa, 24.4, 215.8 g/m² and 370.9 g/m² respectively (Tab 4)
410 and all of which are consistent with the results based on AOD. The CER of ice clouds also shows a consistent
411 decrease by 8.8 μm on the polluted condition based on CDNC. We noticed that the changes of
412 COT/CWP/CER for both liquid and ice based on CDNC are much larger than that based on AOD, which
413 indicates that these cloud properties might be more sensitive to the indicator of CDNC rather than AOD.

414 According to the above comparison, the concurrent changes of cloud properties along with heavy rainfall
415 diurnal variation show consistent results using the two aerosol indicators (AOD and CDNC). The pollution
416 corresponds to the increase of CF, ice COT, liquid and ice CWP, but the decrease of cloud top height (the
417 increase of CTP corresponds to the decrease of cloud top height) and ice CER. The liquid COT and liquid
418 CER are also increased with the enhanced pollution in the AOD analysis. Besides, these above results exhibit
419 significant when we limited the moisture to the dryer condition (SH less than 25th percentile) or intermediate
420 condition (SH more than 25th percentile and less than 75th percentile). When the moisture is higher (SH more
421 than 75th percentile), the change of CTP does not show significant based on CDNC.

422 For these results, we made the following speculation: First, the CF, liquid & ice COT and CWP increase
423 with pollution, might because the aerosols serving as CCN can nucleate a larger number of cloud droplets and
424 accumulate more liquid water in the cloud thus increase the CF, COT and CWP. Second, the CTP increases
425 under pollution using both AOD and CDNC, which denotes the decrease of the cloud top height, might
426 because the earlier start of the precipitation process (Fig. 3) inhibits the vertical growth of clouds. Third, the
427 ice CER decreases under pollution using either AOD or CDNC, probably because the increased cloud droplet
428 number leads to more cloud droplets transforming into ice crystals and causes the decrease of ice CER
429 (Chylek et al., 2006; Zhao et al., 2018; Gryspeerd et al., 2018). However, the results of liquid CER might
430 have uncertainties. The liquid CER is increased when AOD increases (Fig. 9), which might be related to the
431 aerosol humidification effect, the misdetection of AOD and cloud water, and also might result from the earlier
432 formation of the clouds and heavy rainfall on the polluted days. Since we cannot distinguish the liquid part of
433 mix-phased clouds from liquid (warm) clouds in the observation, the above changes of liquid cloud properties
434 might come from both the liquid (warm) clouds and the liquid part of mixed-phase clouds. Likewise, the
435 above-mentioned changes of ice cloud properties might come from both ice (cold) clouds and the ice part of
436 mixed-phase clouds. Currently the detailed physical processes of cold clouds and mixed-phase clouds have
437 been not clarified yet, including the diffusional grow, accretion, riming and melting process of ice
438 precipitation (Cheng et al., 2010), which needs numerical model simulations to be further explored.

439 **4.2 Sensitivities to CCN and moisture**

440 Section 3.3 has shown that the diurnal variation of heavy rainfall with more moisture supply is similar with
441 the changes of heavy rainfall with more sulfate aerosols. We assume that the moisture under the cloud base
442 and the sulfate serving as CCN both influence the cloud properties (Yuan et al., 2008; Jiang et al., 2008; Jung
443 et al., 2013; Qiu et al., 2017). To identify the effect of CCN on clouds and its sensitivity to moisture, using
444 CDNC to represent CCN, we purposely investigated the changes of above cloud properties on the different
445 conditions of the CDNC and the low-level moisture (850hPa SH) respectively.

446 We categorized all cases of heavy rainfall into four groups, which are (1) clean and dry, (2) polluted and
447 dry, (3) clean and wet, (4) polluted and wet, and checked the changes of above cloud properties, as shown in
448 Tab. 5. To retrieve the comparable samples, here “clean/polluted” refers to the CDNC on that day less/more

449 than 25th/75th percentile of the CDNC among the heavy rainfall days, and similarly, the “dry/wet” refers to the
450 SH on that day less/more than 25th/75th percentile of itself among the heavy rainfall days. The average CDNC
451 is 68.58 cm⁻³ on the dry condition and 68.56 cm⁻³ on the wet condition, and the average SH is 11.3 g/kg and
452 11.8 g/kg on the clean and polluted conditions respectively, thus we can consider the CDNC or SH remains
453 the same when the other condition changes. We made the significant test of differences between group 1 and 2,
454 group 1 and 3, group 2 and 4, group 3 and 4. Because the CF is fixed above 80% when calculating the CDNC
455 (see in Sect. 2.1.3), here the selected groups all belong to the condition of higher CF.

456 Comparing the results of group 1 and 2, which are both on the dry condition, we can identify the influence
457 of CDNC on the cloud properties, which stands for the effect of CCN. The changes of these cloud variables
458 are the same as that in Sect. 4.1, that the CF, ice COT and liquid & ice CWP are increased on the polluted
459 condition, while the cloud top height and ice CER are decreased based on CDNC. Among these variables, the
460 ice COT and liquid & ice CWP are especially larger on the polluted condition, which are 5-6 times larger than
461 that on the clean condition (Tab. 5). On the wet condition, comparing the group 3 and 4, the changes are
462 similar that the CF, ice COT and liquid & ice CWP are increased and the ice CER are decreased but the
463 change of CTP becomes not significant. However, the changes of these variables on the dry condition are
464 evidently enhanced than that on the wet condition, which indicates these cloud properties might be more
465 sensitive to CDNC on the dry condition. The above comparisons indicate that with the increase of CDNC
466 (CCN), the CF, ice COT and liquid & ice CWP are increased while the ice CER is decreased regardless of the
467 moisture amount. Although the comparisons of liquid COT and liquid CER based on CDNC are meaningless
468 since the CDNC is calculated by the two variables, we infer that the increase of liquid COT and the decrease
469 of liquid CER (Tab. 5) might be not completely caused by CDNC calculation but the natural effect of CCN.

470 Comparing the results of group 1 and 3, we can get the changes of cloud properties related only to moisture
471 on the same clean condition. A common feature is that CTP, COT and CWP both for liquid and ice exhibit
472 increases along with the increase of moisture. Compared with the CTP on the clean and dry condition, it
473 increases on both polluted & dry condition (group 2) and clean & wet condition (group 3), but on the former
474 condition its increase is larger, which indicates the influence of moisture on CTP might be secondary
475 compared to the CDNC (CCN) effect. Similarly, comparing the COT/CWP in group 2 and 3, the increases of
476 COT and CWP both for liquid and ice in group 2 are 3-6 times larger than that in group 3, which indicates that
477 the influences of moisture on COT and CWP may not overcome the influence of CCN. With the increase of
478 moisture, the change of liquid CER is not significant on the same clean condition, but the ice CER is
479 significantly decreased. On the polluted condition, comparing group 2 and 4, we found the COT and CWP
480 both for liquid and ice on the wet condition are evidently smaller than that on the dry condition, which
481 indicates that increasing the moisture might partly compensate for the influence of CDNC (CCN) on
482 COT/CWP.

483 The results above indicate that both CDNC (CCN) and moisture have impacts on cloud properties. They

484 both contribute to the increase of CF, COT and CWP, in which the influence of CDNC (CCN) on COT and
485 CWP are significantly larger than moisture. The increase of either CDNC or moisture corresponds to the
486 increase of CTP. But when the CDNC and moisture increase simultaneously, the CTP becomes smaller. Both
487 CDNC and moisture correspond to the significant decrease of ice CER, while only CDNC corresponds to the
488 decrease of liquid CER and that might be ascribed to the calculation method of CDNC. To reduce
489 uncertainties, we have tested the SH at different levels (e.g., 700 hPa and 800 hPa) and different moisture
490 indicator (e.g. absolute humidity) to verify these results, and found most cloud variables show the similar
491 changes with above except for the CTP and the liquid CER, which indicates the changes of CTP and liquid
492 CER are more sensitive and have larger uncertainties. Since the behaviors of cloud changes are similar along
493 with the increase of either CDNC (CCN) or moisture but more sensitive to the former, the results in Sect. 4.1
494 might actually reflect the combined effect of CCN and moisture, and the aerosol effect on these cloud
495 properties might be dominant on the polluted days.

496 Therefore, combining with the results in Sect. 3.3, although we cannot completely separate the aerosols and
497 moisture, the CCN is assumed to play a vital role on the clouds and precipitation especially in a relatively dry
498 environment. In the relatively wet environment, the CCN might have some inhibitory effect since the duration
499 of heavy rainfall is shorter with the increase of sulfate when it is extremely wet, and the changes of cloud
500 features along with the CDNC increase are smaller on the wet condition. Due to the limitations of
501 observational study, we currently cannot figure out the respective roles of aerosols and moisture.

502

503 **5. Hypothesis**

504 According to all the above results, we have made hypotheses about the aerosol effects on the heavy rainfall
505 over the BTH region. In Sect. 3.1 we found that the heavy rainfall has earlier start and peak time, and longer
506 duration on the polluted condition. And afterwards, the earlier start of rainfall under pollution was found
507 related to absorbing aerosols mainly referring to BC (Fig. 4a&6a). We also compared the effect of BC on the
508 associated clouds. Figure 10a shows the CF larger than 90% rarely occurs in the more BC environment, which
509 might be associated with the semi-direct effect of BC (Ackerman, 2000) or estimated inversion strength and
510 BC co-vary. This result indicates the influence of BC on the heavy rainfall in Fig. 6a is mainly due to the
511 radiative effect rather than the cloud effect. The mechanism of BC effect on the heavy rainfall can be
512 interpreted by our previous study (Zhou et al., 2018) as: BC absorbs shortwave radiation during the daytime
513 and warms the lower troposphere at around 850 hPa, and then increases the instability of the lower to middle
514 atmosphere (850-500hPa) so that enhances the local upward motion and moisture convergence. As a result,
515 the BC-induced thermodynamic instability of the atmosphere triggers the occurrence of heavy rainfall in
516 advance. Thus, the low-level heating effect of BC might play a dominant role in the beginning of rainfall
517 especially before the formation of clouds during the daytime.

518 The delayed start of heavy rainfall with scattering aerosols in Fig. 4a and more sulfate in Fig. 6b is
519 consistent with many studies that both the radiative effect and cloud effect of sulfate-like aerosols could delay
520 or suppress the occurrence of rainfall (Guo et al., 2013; Wang et al., 2016; Rosenfeld et al. 2014). Sulfate-like
521 aerosols as scattering aerosols could prevent the shortwave radiation from arriving at the surface thus cool the
522 surface and stabilize the atmosphere, which suppresses the rainfall formation (Guo et al., 2013; Wang et al.,
523 2016). Sulfate-like aerosols serving as CCN can also suppress the rainfall by cloud effect through reducing the
524 cloud droplet size and thus suppressing the collision-coalescence process of cloud droplets (Albrecht 1989;
525 Rosenfeld et al. 2014). Figure 10b does shows that in contrast with BC, the CF larger than 90% is
526 significantly increased in the more sulfate environment, which indicates the sulfate-like aerosols might have
527 more evident influence on the clouds and subsequently the rainfall changes associated with sulfate are
528 probably due to the cloud effects. Another significant feature is the longer duration of heavy rainfall in the
529 scattering aerosol cases, more sulfate cases and high moisture cases (Fig 4c, 6b&7a). We speculate that the
530 postponed start of heavy rainfall is mainly due to the effect of sulfate-like aerosols, while the longer duration
531 is caused by both the cloud effect of sulfate-like aerosols and the increased moisture supply, because
532 increasing either CCN or the moisture supply can increase cloud water (Sect. 4.2), which could lead to the
533 longer rainfall duration. To further investigate the mechanism of longer duration, we need the assistance of
534 numerical model simulations in the future work.

535 Accordingly, we speculate that the earlier start time of heavy rainfall related to absorbing aerosols (BC) is
536 due to the radiative heating of absorbing aerosols, while the longer rainfall duration is probably caused by
537 both the cloud effect of sulfate-like aerosols and the increased moisture supply. As a summary we use a
538 schematic diagram (Fig. 11) to illustrate how aerosols modify the heavy rainfall over the BTH region. On one
539 hand, BC heats the lower troposphere, changing the thermodynamic condition of atmosphere, which increases
540 the upward motion and accelerates the formation of clouds and rainfall. On the other hand, the increased
541 upward motion transports more sulfate-like particles and moisture into the clouds so that more CCN and
542 sufficient moisture increase the cloud water, thus might prolong the duration of rainfall. As a result, the heavy
543 rainfall over BTH region in southwesterly shows earlier start and peak time, and longer duration might due to
544 the combined effect of aerosol radiative effect, aerosol cloud effect as well as the moisture effect. To further
545 distinguish the individual effect, we need to conduct numerical model simulations in our future study.

546

547 **6. Conclusions and discussion**

548 **6.1 Conclusions**

549 Using the gauge-based hourly rainfall records, aerosol and cloud satellite products and high temporal
550 resolution reanalysis datasets during 2002-2012, this study investigated the different characteristics of heavy
551 rainfall in the diurnal time scale on the clean and polluted conditions respectively. Based on macro and micro

552 aerosol indicators that are AOD from MODIS aerosol product and calculated CDNC from MODIS cloud
553 product, we found three features of heavy rainfall changing associated with aerosols that the rainfall start and
554 peak time occur earlier and the duration becomes longer. The quantitative differences exist between the two
555 indicators, i.e., the statistic differences of above features between clean and polluted conditions are 0.7, 1.0,
556 0.8 hours based on AOD and 1.4, 3.0, 2.2 hours based on CDNC.

557 The different relationships of absorbing and scattering aerosols to the diurnal shift were also distinguishable
558 using ultraviolet AI from OMI and reanalysis AOD of two aerosol types (BC and sulfate). The absorbing
559 aerosols (BC) correspond to the earlier start and peak time of heavy rainfall, while the scattering aerosols
560 (sulfate) correspond to the delayed start time and the longer duration. Considering that the moisture has
561 indispensable influence on the rainfall, the role of moisture (SH at 850 hPa) on the heavy rainfall is also
562 investigated, which shows similar with the scattering aerosols (sulfate). Further analysis indicates the duration
563 of heavy rainfall is prolonged in the presence of more sulfate on the relatively dry condition but is shortened
564 on the extremely wet condition.

565 By comparing the characteristics of cloud macrophysics and microphysics variables, using both AOD and
566 CDNC we found the CF, ice COT, liquid and ice CWP are increased on the polluted condition, but the cloud
567 top height and the ice CER are reduced. Liquid COT and liquid CER are also increased in AOD analysis.
568 Comparing the influences of CDNC which represents CCN and SH at 850 hPa which represents moisture
569 condition respectively on these cloud variables, the cloud properties show similar changes with the increase of
570 CDNC and moisture, but seem more sensitive to the CDNC (CCN), e.g., the liquid & ice COT and CWP
571 increase more in the environment of high CDNC than that of high SH.

572 According to these results, we speculate that both aerosol radiative effect and cloud effect have impacts on
573 the diurnal variation of heavy rainfall in the BTH region. The heating effect of absorbing aerosols especially
574 BC increases the instability of the lower to middle atmosphere so that generates the heavy rainfall occurrence
575 in advance. And the increased moisture supply and increased aerosols which nucleate more cloud droplets and
576 accumulate more liquid water in clouds, leading to the longer duration of heavy rainfall.

577 **6.2 Discussion**

578 In this study we used two aerosol indicators, AOD and CDNC, which discriminates the pollution levels for
579 different purposes. AOD is a good proxy for the large-scale pollution level, but it stands for the optical feature
580 of aerosols and cannot well represent CCN when we focused on the aerosol-cloud interaction (Shinozuka et al.,
581 2015). CDNC is a better proxy for CCN compared with AOD, which facilitates the study on the cloud changes
582 associated with aerosol pollution. But the retrieved CDNC has larger uncertainties. First, the assumptions in
583 the calculation of CDNC are idealized that CDNC is constant with height in a cloud and cloud liquid water
584 increases monotonically at an adiabatic environment (Grosvenor et al., 2018), but the target of this study is the
585 convective clouds with rainfall that may be not consistent with the adiabatic assumption. Second, as indicated

586 by Grosvenor et al. (2018), the uncertainties in the pixel-level retrievals of CDNC from MODIS with $1^\circ \times 1^\circ$
587 spatial resolution can be above 54%, which come from the uncertainties of parameters and the original COT
588 and CER data using in the calculation, and also the influence of heterogeneity effect from thin clouds. To
589 reduce the influence of heterogeneity effect as much as possible, we have attempted to limit the conditions of
590 CF, liquid COT and CER when calculating CDNC in the study. Besides, this study primarily focuses on the
591 relative changes of CDNC, which may be also influenced by the potential systematic biases in the CDNC
592 calculation, but actually reduced the uncertainties of absolute values. Another problem of CDNC in this study
593 is that the CDNC is actually influenced by updraft velocity when we use CDNC to represent CCN since both
594 CCN and updraft velocity could contribute to aerosol activation and increase CDNC (Reutter et al., 2009). We
595 used the vertical velocity at 850 hPa obtained from ERA-interim reanalysis data to investigate the relationship
596 between CDNC and updraft, and the results show that there is no significant correlation found between CDNC
597 and vertical velocity (among all cases or just polluted cases), although the vertical velocity is larger in the
598 polluted cases. We also checked the results of rainfall based on CDNC when limiting the vertical velocity to a
599 certain range (less than 25th percentile, 25th – 75th percentile or more than 75th percentile), and the main
600 conclusion did not change. Besides, the increase of vertical velocity on the polluted days during daytime we
601 think is related to the pollutants (Zhou et al., 2018), which means the pollutants including the aerosols serving
602 as CCN and the updraft are co-varied and they might be the cause and effect for each other. Therefore, we
603 suppose the CDNC could stand for CCN to a certain extent although it might be partially dependent of updraft
604 velocity.

605 In addition to AOD and CDNC, we also applied ultraviolet AI and AOD of BC/sulfate to identify different
606 types of aerosols. We found that the AI has a weak positive correlation with AOD from MODIS, which
607 indicates the results on absorbing aerosol days might represent the results on polluted days if identified by
608 AOD. To avoid the uncertainty, we re-examined the results using AI when removing the polluted cases
609 identified by AOD, and found the major results are not changed. The comparisons of BC/sulfate AOD cases
610 also have uncertainties because they are retrieved from MACC reanalysis data. Although the above four
611 indicators have their own uncertainties, currently we cannot find more reliable datasets in a long-term
612 observational record. The major findings using these four indices could well identify the changes of rainfall
613 and clouds accompanied with aerosols, but are insufficient to clarify the aerosol effect on clouds and
614 precipitation.

615 This study has clearly identified the relationship of the aerosol pollution and the diurnal changes of heavy
616 rainfall and associated clouds in the BTH region. However, although this work has attempted to exclude the
617 impacts from the meteorological background particularly circulation and moisture, the observation study still
618 has its limitations on studying aerosol effects on rainfall and clouds: first, the noise and uncertainty of
619 different observational data cannot be avoid, e.g., the misdetection of CF in the satellite product when AOD is
620 large (Brennan et al., 2005; Levy et al., 2013) and the mutual interference between liquid and ice clouds (Holz
621 et al., 2008; Platnick et al., 2017); Second, the meteorological co-variations cannot be completely removed

622 thus bring the uncertainties, e.g., the meteorology might have a vital influence on the relationship of AOD and
623 CF (Quaas et al., 2010; Grandey et al., 2013) and the relationship of AOD and CTP (Gryspeerd et al., 2014a);
624 Third, the different types of aerosols cannot be completely separated, although we used AI index and AOD of
625 BC/sulfate to distinguish the respective effects of absorbing aerosols and scattering aerosols. In addition, we
626 selected the extreme ranges of AOD/CDNC to compare the characteristics of heavy rainfall and associated
627 clouds, which could bring uncertainties that these extreme conditions might be related with totally different
628 microphysical process or meteorological background. So we further checked the results using the middle
629 range of AOD and CDNC such as 25th – 50th percentile versus 50th -75th percentile. The results are basically
630 the same and significant except the change of the peak time of heavy rainfall is not significant based on AOD.
631 The influence of aerosol pollution on the heavy rainfall and clouds may not be linear, but this study using the
632 idea of comparative experiments gives the observational results of the relationships between them. Numerical
633 model simulations are necessarily applied to further study the specific impact of aerosols on the heavy rainfall.
634 And the detailed processes of aerosol effect on the precipitation formation of mix-phased clouds also needs
635 further exploration in our future study.

636

637 **Data availability**

638 We are grateful to the National Meteorological Information Centre (NMIC) of the China Meteorological
639 Administration (CMA) for providing hourly precipitation datasets. MODIS aerosol and cloud data were
640 obtained from <http://ladsweb.modaps.eosdis.nasa.gov>; ultraviolet AI data from OMI was obtained from
641 <https://daac.gsfc.nasa.gov/datasets?keywords=OMI&page=1>; MACC-II and ERA-interim reanalysis datasets
642 were obtained from <http://apps.ecmwf.int/datasets>.

643 **Author contributions**

644 JY and SZ conceived the study. SZ processed data and drew the figures. SZ and JY analyzed the observational
645 results and WCW, CZ and DG gave the professional guidance. PS provided the hourly precipitation dataset.
646 SZ and JY prepared the manuscript with contributions from WCW and CZ.

647 **Competing interests**

648 The authors declare that they have no conflict of interest.

649 **Acknowledgements**

650 Jing Yang, Daoyi Gong & Peijun Shi are supported by funds from the National Natural Science Foundation of
651 China (41621061 and 41775071) and the National Key Research and Development Program-Global Change
652 and Mitigation Project: Global Change Risk of Population and Economic System: Mechanism and
653 Assessment (2016YFA0602401), Siyuan Zhou is supported by funds from State Key Laboratory of Earth

654 Surface Processes and Resource Ecology and Key Laboratory of Environmental Change and Natural Disaster.
655 Wei-Chyung Wang acknowledges the support of grants (to SUNYA) from the Office of Sciences (BER), U.S.
656 DOE and the U.S. National Science Foundation (1545917) in support of the Partnership for International
657 Research and Education project at the University at Albany. We deeply appreciate two anonymous referees
658 for their in-depth comments and constructive suggestions.

659

660 **References:**

- 661 Ackerman, A. S.: Reduction of Tropical Cloudiness by Soot, *Science*, 288, 1042-1047,
662 doi:10.1126/science.288.5468.1042, 2000.
- 663 Albrecht, B. A.: Aerosols, cloud microphysics, and fractional cloudiness, *Science*, 245, 1227-1230,
664 doi:10.1126/science.245.4923.1227, 1989.
- 665 Altaratz, O., Bar-Or, R. Z., Wollner, U., and Koren, I.: Relative humidity and its effect on aerosol optical
666 depth in the vicinity of convective clouds, *Environ. Res. Lett.*, 8, 034025,
667 doi:10.1088/1748-9326/8/3/034025, 2013.
- 668 Anonymous: Atmospheric Sciences Thesaurus, China Meteorological Press: Beijing, China, 1994. (in
669 Chinese)
- 670 Anonymous: IPCC fifth assessment report, *Weather*, 68, 310-310, 2013.
- 671 Bellouin, N., Quaas, J., Morcrette J. -J., and Boucher, O.: Estimates of aerosol radiative forcing from the
672 MACC re-analysis, *Atmos. Chem. Phys.*, 13, 2045-2062, doi:10.5194/acp-13-2045-2013, 2013.
- 673 Benedetti, A., Morcrette, J. J., Boucher, O., Dethof, A., Engelen, R. J., Fisher, M., Flentje, H., Huneeus, N.,
674 Jones, L., Kaiser, J. W., Kinne, S., Mangold, A., Razinger, M., Simmons, A. J., and Suttie, M.: Aerosol
675 analysis and forecast in the European Centre for Medium-Range Weather Forecasts Integrated Forecast
676 System: 2. Data assimilation, *J. Geophys. Res.*, 114, D13205, doi:10.1029/2008JD011115, 2009.
- 677 Brennan, J., Kaufman, Y., Koren, I., and Rong, L.: Aerosol-cloud interaction-Misclassification of MODIS
678 clouds in heavy aerosol, *IEEE T. Geosci. Remote*, 43, 911–915, doi:10.1109/TGRS.2005.844662, 2005.
- 679 Bennartz, R., and Rausch, J.: Global and regional estimates of warm cloud droplet number concentration
680 based on 13 years of AQUA-MODIS observations, *Atmos. Chem. Phys.*, 17, 9815-9836,
681 doi:10.5194/acp-17-9815-2017, 2017.
- 682 Bennartz, R.: Global assessment of marine boundary layer cloud droplet number concentration from satellite, *J.*
683 *Geophys. Res.*, 112, D02201, doi:10.1029/2006JD007547, 2007.
- 684 Boers, R., Acarreta, J. A., and Gras, J. L.: Satellite monitoring of the first indirect aerosol effect: Retrieval of
685 the droplet concentration of water clouds, *J. Geophys. Res.*, 111, D22208, doi:10.1029/2005JD006838,
686 2006.
- 687 Boucher, O., and Quaas, J.: Water vapour affects both rain and aerosol optical depth, *Nat. Geosci.*, 6, 4-5,
688 doi:10.1038/ngeo1692, 2012.
- 689 Chen, Q., Yin, Y., Jin, L., Xiao, H., and Zhu, S.: The effect of aerosol layers on convective cloud

690 microphysics and precipitation, *Atmos. Res.*, 101, 327-340, doi:10.1016/j.atmosres.2011.03.007, 2011.

691 Cheng, C. T., Wang, W. C., and Chen, J. P.: A modeling study of aerosol impacts on cloud microphysics and
692 radiative properties, *Q. J. R. Meteorol. Soc.*, 133, 283–297, doi:10.1002/qj.25, 2007.

693 Cheng, C. T., Wang, W. C., and Chen, J. P.: Simulation of the effects of increasing cloud condensation nuclei
694 on mixed-phase clouds and precipitation of a front system, *Atmos. Res.*, 96, 461-476, doi:
695 10.1016/j.atmosres.2010.02.005, 2010.

696 Chylek, P., Dubey, M. K., Lohmann, U., Ramanathan, V., Kaufman, Y. J., Lesins, G., Hudson, J., Altmann,
697 G., and Olsen, S.: Aerosol indirect effect over the Indian Ocean, *Geophys. Res. Lett.*, 33, L06806,
698 doi:10.1029/2005GL025397, 2006.

699 Dee, D. P., Uppala, S. M., Simmons, A. J., Berrisford, P., Poli, P., Kobayashi, S., Andrae, U., Balmaseda, M.
700 A., Balsamo, G., Bauer, P., Bechtold, P., Beljaars, A. C. M., van de Berg, L., Bidlot, J., Bormann, N.,
701 Delsol, C., Dragani, R., Fuentes, M., Geer, A. J., Haimberger, L., Healy, S. B., Hersbach, H., Hólm, E.
702 V., Isaksen, I., Kållberg, P., Köhler, M., Matricardi, M., McNally, A. P., Monge-Sanz, B. M.,
703 Morcrette, J.-J., Park, B.-K., Peubey, C., de Rosnay, P., Tavolato, C., Thépaut, J.-N., Vitart, F.: The
704 ERA-Interim reanalysis: configuration and performance of the data assimilation system, *Q. J. R.*
705 *Meteorol. Soc.*, 137, 553–597, doi:10.1002/qj.828, 2011.

706 Fan, J. W., Rosenfeld, D., Yang, Y., Zhao, C., Leung, L. R., and Li, Z. Q.: Substantial contribution of
707 anthropogenic air pollution to catastrophic floods in Southwest China, *Geophys. Res. Lett.*, 42,
708 6066-6075, doi:10.1002/2015GL064479, 2015.

709 Garrett, T. J. and Zhao, C.: Increased Arctic cloud longwave emissivity associated with pollution from
710 mid-latitudes, *Nature*, 440, 787-789, doi:10.1038/nature04636, 2006.

711 Givati, A., and Rosenfeld, D.: Quantifying precipitation suppression due to air pollution, *J. Appl. Meteor.*, 43,
712 1038-1056, doi:10.1175/1520-0450(2004)043<1038:QPSDTA>2.0.CO;2, 2004.

713 Grandey, B. S., and Stier, P.: A critical look at spatial scale choices in satellite-based aerosol indirect effect
714 studies, *Atmos. Chem. Phys.*, 10, 11459–11470, doi:10.5194/acp-10-11459-2010, 2010.

715 Grandey, B. S., Stier, P. and Wagner, T. M.: Investigating relationships between aerosol optical depth and
716 cloud fraction using satellite, aerosol reanalysis and general circulation model data, *Atmos. Chem. Phys.*,
717 13, 3177-3184, doi:10.5194/acp-13-3177-2013, 2013.

718 Gryspeerdt, E., Sourdeval, O., Quaas, J., Delanoë, J., Krämer, M., and Kühne, P.: Ice crystal number
719 concentration estimates from lidar–radar satellite remote sensing – Part 2: Controls on the ice crystal
720 number concentration, *Atmos. Chem. Phys.*, 18, 14351–14370, doi:10.5194/acp-18-14351-2018, 2018.

721 Gryspeerdt, E., Stier, P., and Grandey, B. S.: Cloud fraction mediates the aerosol optical depth-cloud top
722 height relationship, *Geophys. Res. Lett.*, 41, 3622-3627, doi:10.1002/2014GL059524, 2014a.

723 Gryspeerdt, E., Stier, P., and Partridge, D. G.: Links between satellite-retrieved aerosol and precipitation,
724 *Atmos. Chem. Phys.*, 14, 9677–9694, doi:10.5194/acp-14-9677-2014, 2014b.

725 Gunthe, S. S., Rose, D., Su, H., Garland, R. M., Achtert, P., Nowak, A., Wiedensohler, A., Kuwata, M.,

726 Takegawa, N., Kondo, Y., Hu, M., Shao, M., Zhu, T., Andreae, M. O., and Poschl, U.: Cloud
727 condensation nuclei (CCN) from fresh and aged air pollution in the megacity region of Beijing, *Atmos.*
728 *Chem. Phys.*, 11, 11023-11039, doi:10.5194/acp-11-11023-2011, 2011.

729 Guo, C. W., Xiao, H., Yang, H. L., and Tang, Q.: Observation and modeling analyses of the macro-and
730 microphysical characteristics of a heavy rain storm in Beijing, *Atmos. Res.*, 156, 125-141,
731 doi:10.1016/j.atmosres.2015.01.007, 2015.

732 Guo, J. P., Deng, M. J., Lee, S. S., Wang, F., Li, Z. Q., Zhai, P. M., Liu, H., Lv, W., Yao, W., and Li, X. W.:
733 Delaying precipitation and lightning by air pollution over the Pearl River Delta, Part I: Observational
734 analyses. *J. Geophys. Res.*, 121, 6472-6488, doi:10.1002/2015JD023257, 2016.

735 Guo, L., Highwood, E. J., Shaffrey, L. C., and Turner, A. G.: The effect of regional changes in anthropogenic
736 aerosols on rainfall of the East Asian Summer Monsoon, *Atmos. Chem. Phys.*, 13, 1521-1534,
737 doi:10.5194/acp-13-1521-2013, 2013.

738 Guo, X. L., Fu, D. H., Guo, X., and Zhang, C. M.: A case study of aerosol impacts on summer convective
739 clouds and precipitation over northern China, *Atmos. Res.*, 142, 142-157,
740 doi:10.1016/j.atmosres.2013.10.006, 2014.

741 Hammer, M. S., Martin, R. V., Li, C., Torres, O., Manning, M., and Boys, B. L.: Insight into global trends in
742 aerosol composition from 2005 to 2015 inferred from the OMI Ultraviolet Aerosol Index, *Atmos. Chem.*
743 *Phys.*, 18, 8097-8112, doi:10.5194/acp-18-8097-2018, 2018.

744 Harikishan, G., Padmakumari, B., Maheskumar, R. S., Pandithurai, G., and Min, Q. L.: Aerosol indirect effects
745 from ground-based retrievals over the rain shadow region in Indian subcontinent, *J. Geophys. Res.*, 121,
746 2369-2382, doi:10.1002/2015JD024577, 2016.

747 Higgins, R. W., Yao, Y., Yarosh, E. S., Janowiak, J. E. and Mo, K. C.: Influence of the Great Plains low-level
748 jet on summertime precipitation and moisture transport over the central United States, *J. Climate*, 10,
749 481-507, doi:10.1175/1520-0442(1997)010<0481:IOTGPL>2.0.CO;2, 1997.

750 Holz, R. E., Ackerman, S. A., Nagle, F. W., Frey, R., Dutcher, S., Kuehn, R. E., Vaughan, M. A., and Baum,
751 B.: Global Moderate Resolution Imaging Spectroradiometer (MODIS) cloud detection and height
752 evaluation using CALIOP, *J. Geophys. Res.*, 113, D00A19, doi: 10.1029/2008JD009837, 2008.

753 Jacobson, M. Z.: Strong radiative heating due to the mixing state of black carbon in atmospheric aerosols,
754 *Nature*, 409, 695-697, doi:10.1038/35055518, 2001.

755 Jiang, H., Feingold, G., and Cotton, W. R.: Simulations of aerosol-cloud-dynamical feedbacks resulting from
756 entrainment of aerosol into the marine boundary layer during the Atlantic Stratocumulus Transition
757 Experiment, *J. Geophys. Res.*, 107(D24), 4813, doi:10.1029/2001JD001502, 2002.

758 Jiang, J. H., Su, H., Schoeberl, M. R., Massie, S. T., Colarco, P., Platnick, S., and Livesey, N. J.: Clean and
759 polluted clouds: Relationships among pollution, ice clouds, and precipitation in South America, *Geophys.*
760 *Res. Lett.*, 35, L14804, doi: 10.1029/2008GL034631, 2008.

761 Jiang, M. J., Li, Z. Q., Wan, B. C., and Cribb, M.: Impact of aerosols on precipitation from deep convective

762 clouds in eastern China, *J. Geophys. Res.*, 121, 9607-9620, doi:10.1002/2015JD024246, 2016.

763 Johnson, D. B.: The role of giant and ultra-giant aerosol particles in warm rain initiation, *J. Atmos. Sci.*, 39,
764 448–460, doi:10.1175/1520-0469(1982)039<0448:TROGAU>2.0.CO;2, 1982.

765 Jung, W. S., Panicker, A. S., Lee, D. I., and Park, S. H.: Estimates of aerosol indirect effect from Terra
766 MODIS over Republic of Korea, *Advances in Meteorology*, 2013 (976813), 1-8,
767 doi:10.1155/2013/976813, 2013.

768 Kim, K. –M., Lau, K. M., Sud, Y. C., and Walker, G. K.: Influence of aerosol radiative forcings on the diurnal
769 and seasonal cycles of rainfall over West Africa and Eastern Atlantic Ocean using GCM simulation, *Clim.*
770 *Dyn.*, 35, 115-126, doi: 10.1007/s00382-010-0750-1, 2010.

771 Lau, K. M., Kim, M. K., and Kim, K. M.: Asian summer monsoon anomalies induced by aerosol direct
772 forcing: the role of the Tibetan Plateau, *Clim. Dyn.*, 26, 855-864, doi:10.1007/s00382-006-0114-z, 2006.

773 Lee, S. S., Donner, L. J., and Phillips, V. T. J.: Impacts of aerosol chemical composition on microphysics and
774 precipitation in deep convection, *Atmos. Res.*, 94, 220-237, doi:10.1016/j.atmosres.2009.05.015, 2009.

775 Lee, S. S., Guo, J., and Li, Z.: Delaying precipitation by air pollution over the Pearl River Delta: 2. Model
776 simulation, *J. Geophys. Res.*, 121, 11739-11760, doi:10.1002/2015JD024362, 2016.

777 Lelieveld, J. and Heintzenberg, J.: Sulfate cooling effect on climate through in-cloud oxidation of
778 anthropogenic SO₂, *Science*, 258, 117-120, doi:10.1126/science.258.5079.117, 1992.

779 Levy, R. C., Mattoo, S., Munchak, L. A., Remer, L. A., Sayer, A. M., Patadia, F., and Hsu, N. C.: The
780 Collection 6 MODIS aerosol products over land and ocean, *Atmos. Meas. Tech.*, 6, 2989–3034,
781 doi:10.5194/amt-6-2989-2013, 2013.

782 Li, H., Cui, X., Zhang, W., and Qiao, L.: Observational and dynamic downscaling analysis of a heavy rainfall
783 event in Beijing, China during the 2008 Olympic Games, *Atmos. Sci. Lett.*, 17, 368-376,
784 doi:10.1002/asl.667, 2016.

785 Li, Z., Niu, F., Fan, J., Liu, Y., Rosenfeld, D., and Ding, Y.: Long-term impacts of aerosols on the vertical
786 development of clouds and precipitation, *Nat. Geosci.*, 4, 888-894, doi:10.1038/ngeo1313, 2011.

787 Lim, K. S. and Hong, S.: Investigation of aerosol indirect effects on simulated flash-flood heavy rainfall over
788 Korea, *Meteor. Atmos. Phys.*, 118, 199-214, doi:10.1007/s00703-012-0216-6, 2012.

789 Liu, G., Shao, H., Coakley Jr. J. A., Curry, J. A., Haggerty, J. A., and Tschudi, M. A.: Retrieval of cloud
790 droplet size from visible and microwave radiometric measurements during INDOEX: Implication to
791 aerosols' indirect radioactive effect, *J. Geophys. Res.*, 108(D1), 4006, doi:10.1029/2001JD001395, 2003.

792 Liu, J., Wang, S., Zhang, W., and Wei, X.: Mechanism analysis of a strong convective weather in Hebei
793 Province, *Advances in Marine Science*, 30, 9-16, 2012. (in Chinese)

794 Menzel, W. P., Frey, R. A., Zhang, H., Wylie, D. P., Moeller, C. C., Holz, R. E., Maddux, B., Baum, B. A.,
795 Strabala, K. I., and Gumley, L. E.: MODIS global cloud-top pressure and amount estimation: Algorithm
796 description and results, *J. Appl. Meteorol. Clim.*, 47, 1175-1198, doi: 10.1175/2007JAMC1705.1, 2008.

797 Min, Q., Joseph, E., Lin, Y., Min, L., Yin, B., Daum, P. H., Kleinman, L. I., Wang, J., and Lee, Y. –N.:

798 Comparison of MODIS cloud microphysical properties with in-situ measurements over the Southeast
799 Pacific, *Atmos. Chem. Phys.*, 12, 11261-11273, doi:10.5194/acp-12-11261-2012, 2012.

800 Nakajima, T. and King, M. D.: Determination of the optical thickness and effective particle radius of clouds
801 from reflected solar radiation measurements. Part I: Theory, *J. Atmos. Sci.*, 47, 1878-1893,
802 doi:10.1175/1520-0469(1990)047<1878:DOTOTA>2.0.CO;2, 1990.

803 Panicker, A. S., Pandithurai, G., and Dipu, S.: Aerosol indirect effect during successive contrasting monsoon
804 seasons over Indian subcontinent using MODIS data, *Atmos. Environ.*, 44, 1937-1943,
805 doi:10.1016/j.atmosenv.2010.02.015, 2010.

806 Platnick, S., Meyer, K., King, M. D., Wind, G., Amarasinghe, N., Marchant, B., Arnold, G. T., Zhang, Z.,
807 Hubanks, P. A., Holz, R. E., Yang, P., Ridgway, W. L., and Riedi, J.: The MODIS cloud optical and
808 microphysical products: Collection 6 updates and examples from Terra and Aqua, *IEEE Trans. Geosci.*
809 *Remote Sens.*, 55, 502-525, doi:10.1109/TGRS.2016.2610522, 2017.

810 Qian, Y., Gong, D. Y., Fan, J. W., Leung, L. R., Bennartz, R., Chen, D. L., Wang, W. G.: Heavy pollution
811 suppresses light rain in China: Observations and modeling, *J. Geophys. Res.*, 114, D00K02,
812 doi:10.1029/2008JD011575, 2009.

813 Qiu, Y., Zhao, C., Guo, J., and Li, J.: 8-Year ground-based observational analysis about the seasonal variation
814 of the aerosol-cloud droplet effective radius relationship at SGP site, *Atmos. Environ.*, 164, 139-146,
815 doi:10.1016/j.atmosenv.2017.06.002, 2017.

816 Quaas, J., Boucher, O., Bellouin, N. and Kinne, S.: Satellite-based estimate of the direct and indirect aerosol
817 climate forcing, *J. Geophys. Res.*, 113, D05204, doi:10.1029/2007JD008962, 2008.

818 Quaas, J., Stevens, B., Stier, P., and Lohmann U.: Interpreting the cloud cover aerosol optical depth
819 relationship found in satellite data using a general circulation model, *Atmos. Chem. Phys.*, 10, 6129-6135,
820 doi:10.5194/acp-10-6129-2010, 2010.

821 Reutter, P., Su, H., Trentmann, J., Simmel, M., Rose, D., Gunthe, S. S., Wernli, H., Andreae, M. O., and
822 Po ¨schl, U.: Aerosol- and updraft-limited regimes of cloud droplet formation: influence of particle
823 number, size and hygroscopicity on the activation of cloud condensation nuclei (CCN), *Atmos. Chem.*
824 *Phys.*, 9, 7067-7080, doi:10.5194/acp-9-7067-2009, 2009.

825 Rienecker, M. M., Suarez, M. J., Todling, R., Bacmeister, J., Takacs, L., Liu, H. C., Gu, W., Sienkiewicz, M.,
826 Koster, R. D., Gelaro, R., Stajner, I., Nielsen, J. E.: The GEOS-5 Data Assimilation
827 System—Documentation of Versions 5.0.1 and 5.1.0, and 5.2.0. NASA Technical Report Series on
828 Global Modeling and Data Assimilation NASA/TM-2008 -104606 27: 92 pp, 2008.

829 Rosenfeld, D.: TRMM observed first direct evidence of smoke from forest fires inhibiting rainfall, *Geophys.*
830 *Res. Lett.*, 26, 3105–3108, doi:10.1029/1999GL006066, 1999.

831 Rosenfeld, D., Lohmann, U., Raga, G. B., O'Dowd, C. D., Kulmala, M., Fuzzi, S., Reissell, A., Andreae, M.
832 O.: Flood or drought: How do aerosols affect precipitation? *Science*, 321, 1309-1313,
833 doi:10.1126/science.1160606, 2008.

834 Rosenfeld, D., Sherwood, S., Wood, R., and Donner, L.: Climate effects of aerosol-cloud interactions, *Science*,
835 343, 379-380, doi:10.1126/science.1247490, 2014.

836 Rosenfeld, D., and Woodley, W. L.: Convective clouds with sustained highly supercooled liquid water down
837 to -37.5°C , *Nature*, 405, 440-442, doi:10.1038/35013030, 2000.

838 Sassen, K., Starr, D., Mace, G. G., Poellot, M. R., Melfi, S. H., Eberhard, W.L., Spinhirne, J. D., Eloranta, E.
839 W., Hagan, D. E., and Hallett, J.: The 5-6 December 1991 FIRE IFO II jet stream cirrus case study:
840 Possible influences of volcanic aerosols, *J. Atmos. Sci.*, 52, 97-123, doi:10.1175/1520-0469(1995)
841 052<0097:TDFIJJ>2.0.CO;2, 1995.

842 Shen, Y., Xiong, A., Wang, Y., and Xie, P.: Performance of high-resolution satellite precipitation products
843 over China, *J. Geophys. Res.*, 115, D02114, doi:10.1029/2009JD012097, 2010.

844 Sherwood, S.: Aerosols and ice particle size in tropical cumulonimbus, *J. Clim.*, 15, 1051-1063,
845 doi:10.1175/1520-0442(2002)015<1051:AAIPSI>2.0.CO;2, 2002.

846 Shinozuka, Y., Clarke, A. D., Nenes, A., Jefferson, A., Wood, R., McNaughton, C. S., Ström, J., Tunved, P.,
847 Redemann, J., Thornhill, K. L., Moore, R. H., Latham, T. L., Lin, J. J., and Yoon, Y. J.: The relationship
848 between cloud condensation nuclei (CCN) concentration and light extinction of dried particles:
849 indications of underlying aerosol processes and implications for satellite-based CCN estimates, *Atmos.*
850 *Chem. Phys.*, 15, 7585-7604, doi:10.5194/acp-15-7585-2015, 2015.

851 Song, X. L. and Zhang, G. J.: Microphysics parameterization for connective clouds in a global climate model:
852 Description and single-column model tests, *J. Geophys. Res.*, 116, D02201, doi:10.1029/2010JD014833,
853 2011.

854 Squires, P.: The growth of cloud drops by condensation: I. general characteristics, *Aust. J. Sci. Res., Ser. A*, 5,
855 66-86, 1952.

856 Squires, P., and Twomey, S.: A comparison of cloud nucleus measurements over central North America and
857 Caribbean Sea, *J. Atmos. Sci.*, 23, 401-404, doi: 10.1175/1520-0469(1966)023<0401:ACOCNM>
858 -2.0.CO;2, 1966.

859 Sun, Y. L., Wang, Z. F., Du, W., Zhang, Q., Wang, Q. Q., Fu, P. Q., Pan, X. L., Li, J., Jayne, J., and Worsnop,
860 D. R.: Long-term real-time measurements of aerosol particle composition in Beijing, China: seasonal
861 variations, meteorological effects, and source analysis, *Atmos. Chem. Phys.*, 15, 10149-10165,
862 doi:10.5194/acp-15-10149-2015, 2015.

863 Tariq, S., and Ali, M.: Spatio-temporal distribution of absorbing aerosols over Pakistan retrieved from OMI on
864 board Aura Satellite, *Atmos. Pollution Res.*, doi: 10.5094/APR.2015.030, 2015.

865 Tao, M. H., Chen, L. F., Wang, Z. F., Tao, J. H., Che, H. Z., Wang, X. H., and Wang, Y.: Comparison and
866 evaluation of the MODIS Collection 6 aerosol data in China, *J. Geophys. Res.*, 120, 6992-7005,
867 doi:10.1002/2015JD023360, 2015.

868 Tao, W. K., Chen, J. P., Li, Z., Wang, C., and Zhang C.: Impact of aerosols on convective clouds and
869 precipitation, *Rev. Geophys.*, 50, RG2001/2012, 1-62, doi: 10.1029/2011RG000369, 2012.

870 Torres, O., Bhartia, P.K., Herman, J.R., Ahmad, Z., Gleason, J.: Derivation of aerosol properties from satellite
871 measurements of backscattered ultraviolet radiation: Theoretical basis, *J. Geophys. Res.*, 103, 17099–
872 17110, doi:10.1029/98JD00900, 1998.

873 Twohy, C. H., Coakley, J. A., and Tahnk, W. R.: Effect of changes in relative humidity on aerosol scattering
874 near clouds, *J. Geophys. Res.*, 114, D05205, doi:10.1029/2008JD010991, 2009.

875 Twomey, S.: The influence of pollution on the shortwave albedo of clouds, *J. Atmos. Sci.*, 34, 1149–1152,
876 doi:10.1175/1520-0469(1977)034<1149:TIOPOT>2.0.CO;2, 1977.

877 Wang, J., Feng, J., Wu, Q., and Z. Yan, Z.: Impact of anthropogenic aerosols on summer precipitation in the
878 Beijing-Tianjin-Hebei urban agglomeration in China: Regional climate modeling using WRF-Chem, *Adv.*
879 *Atmos. Sci.*, 33, 753-766, doi:10.1007/s00376-015-5103-x, 2016.

880 Wolyn, P. G., and Mckee, T. B.: The mountain plains circulation east of a 2-km-high north south barrier, *Mon.*
881 *Weather Rev.*, 122, 1490-1508, doi:10.1175/1520-0493(1994)122<1490:TMPCEO>2.0.CO;2, 1994.

882 Wu, P., Ding, Y. H., and Liu, Y. J.: Atmospheric circulation and dynamic mechanism for persistent haze
883 events in the Beijing-Tianjin-Hebei region, *Adv. Atmos. Sci.*, 34, 429-440,
884 doi:10.1007/s00376-016-6158-z, 2017.

885 Yang, X., Zhao, C., Zhou, L., Li, Z., Cribb, M., and Yang, S.: Wintertime cooling and a potential connection
886 with transported aerosols in Hong Kong during recent decades, *Atmos. Res.*, 211, 52-61,
887 doi:10.1016/j.atmosres.2018.04.029, 2018.

888 Yu, R. C., Zhou, T. J., Xiong, A. Y., Zhu, Y. J., and Li, J. M.: Diurnal variations of summer precipitation over
889 contiguous China, *Geophys. Res. Lett.*, 34, L017041, doi:10.1029/2006GL028129, 2007.

890 Yuan, T., Li, Z., Zhang, R., and Fan, J.: Increase of cloud droplet size with aerosol optical depth: An
891 observation and modeling study, *J. Geophys. Res.*, 113, D04201, doi:10.1029/2007JD008632, 2008.

892 Yuan, W. H., Yu, R. C., Chen, H. M., Li, J., and Zhang, M. H.: Subseasonal Characteristics of Diurnal
893 Variation in Summer Monsoon Rainfall over Central Eastern China, *J. Climate*, 23, 6684-6695,
894 doi:10.1175/2010JCLI3805.1, 2010.

895 Zeng, S., Riedi, J., Trepte, C. R., Winker, D. M., and Hu, Y. -X.: Study of global cloud droplet number
896 concentration with A-Train satellites, *Atmos. Chem. Phys.*, 14, 7125-7134, doi:
897 10.5194/acp-14-7125-2014, 2014.

898 Zhao, B., Gu, Y., Liou, K. -N., Wang, Y., Liu, X., Huang, L., Jiang, J. H., and Su, H.: Type-Dependent
899 Responses of Ice Cloud Properties to Aerosols From Satellite Retrievals, *Geophys. Res. Lett.*, 45, 3297–
900 3306, doi:10.1002/2018GL077261, 2018.

901 Zhou, S., Yang, J., Wang, W. C., Gong, D., Shi, P., and Gao, M.: Shift of daily rainfall peaks over the
902 Beijing–Tianjin–Hebei region: An indication of pollutant effects? *Int. J. Climatol.* 2018;1–10,
903 doi:10.1002/joc.5700, 2018.

904 Zhu, Y., Rosenfeld, D., and Li, Z.: Under what conditions can we trust retrieved cloud drop concentrations in
905 broken marine stratocumulus? *J. Geophys. Res.*, 123, 8754-8767, doi:10.1029/2017JD028083, 2018.

906

907 **Tables**

908

Indicator	Source	Begin time	Thresholds	
			25 th percentile	75 th percentile
AOD	MODIS	2002	0.98	2.00
CDNC (cm ⁻³)	MODIS	2002	30.10	91.03
AAI	OMI	2005	0.13	0.52
SAI	OMI	2005	- 0.13	- 0.35
AOD of BC	MACC	2003	0.04	0.06
AOD of sulfate	MACC	2003	0.46	0.87
SH at 850 hPa (g/kg)	ERA-interim	2002	9.96	12.95

909

910 Table 1. The indicators of aerosols and moisture used in the study and their sources, begin times and the
 911 thresholds (25th and 75th percentiles). The end time of all data is to 2012.

912

913

914

915

Characteristics of heavy rainfall	Clean		Polluted		Difference		Significance	
	AOD	CDNC	AOD	CDNC	AOD	CDNC	AOD	CDNC
Start time	24.2 (3.9)	24.3 (4.0)	23.5 (4.8)	22.9 (3.9)	- 0.7	- 1.4	P<0.05	P<0.05
Peak time	23.0 (4.0)	22.1 (5.3)	22.0 (4.8)	19.1 (5.7)	- 1.0	- 3.0	P<0.05	P<0.05
Duration	4.0 (2.1)	5.5 (3.3)	4.8 (2.8)	7.7 (4.3)	0.8	2.2	P<0.05	P<0.05
Intensity	164.9 (98.4)	166.0 (89.3)	169.6 (94.3)	162.7 (89.1)	4.7	- 3.3	P>0.1	P>0.1

916

917 Table 2. The mean values of start time (units: LST), peak time (units: LST), duration (units: hours) and
 918 intensity (units: 0.1mm/hour) of heavy rainfall respectively on the clean and polluted conditions using two
 919 indicators of AOD and CDNC, and their differences (polluted minus clean) and significances. The numbers in
 920 the brackets stand for the standard deviations on the means. “P<0.05” stands for the difference has passed the
 921 significance test of 95%, and “P>0.1” stands for the difference did not pass the significance test of 90%.

922

923

Characteristics of heavy rainfall	AAI	SAI	Difference (AAI-SAI)	Less BC	More BC	Difference (More-Less)	Less sulfate	More sulfate	Difference (More-Less)
Start time	23.4 (4.8)	24.1 (4.4)	-0.7	24.2 (4.8)	23.9 (4.4)	-0.3	24.0 (4.3)	24.5 (4.4)	0.5
Peak time	21.0 (5.3)	22.6 (5.1)	-1.6	23.4 (5.3)	22.3 (4.0)	-1.1	23.2 (4.5)	22.9 (4.8)	-0.3
Duration	5.0 (3.1)	6.0 (3.8)	-1.0	4.8 (2.6)	4.6 (2.7)	-0.2	4.0 (2.1)	5.5 (3.0)	1.5

924

925 Table 3. The mean values of start time (units: LST), peak time (units: LST) and duration (units: hours) of
926 heavy rainfall respectively on the conditions with more absorbing aerosols (AAI more than 75th percentile,
927 from OMI), more scattering aerosols (SAI more than 75th percentile, from OMI), less or more BC (AOD of
928 BC less than 25th or more than 75th percentile, from MACC), less or more sulfate (AOD of sulfate less than
929 25th or more than 75th percentile, from MACC), and their differences. Numbers in the brackets stand for the
930 standard deviations on the means. All differences have passed the significant test of 95%.

931

932

933

934

Clean/Polluted	CF	CTP	COT		CWP		CER		
			liquid	ice	liquid	ice	liquid	ice	
AOD	Clean	62.8 (17.6)	442.3 (149.6)	6.9 (4.5)	6.7 (8.5)	62.8 (36.6)	123.1 (168.9)	16.7 (4.4)	32.0 (8.7)
	Polluted	89.3 (12.9)	487.3 (145.7)	10.0 (5.8)	12.9 (17.0)	96.4 (52.5)	211.3 (279.3)	17.5 (3.5)	29.2 (9.0)
CDNC	Clean	94.5 (6.1)	398.0 (131.7)	8.1 (6.0)	8.7 (10.6)	102.4 (104.3)	171.6 (204.3)	20.4 (2.8)	34.2 (6.0)
	Polluted	97.4 (4.2)	430.8 (135.2)	40.4 (21.5)	33.1 (22.7)	318.2 (213.2)	542.5 (447.8)	12.2 (1.9)	25.4 (8.7)

935

936 Table 4. The mean values of CF (units: %), CTP (units: hPa), COT (liquid and ice, units: none), CWP (liquid
937 and ice, units: g/m²) and CER (liquid and ice, units: μm) from MODIS C6 cloud product on the clean
938 condition (less than 25th percentile) and polluted condition (more than 75th percentile) using two indicators of
939 AOD and CDNC. Numbers in the brackets stand for the standard deviations on the means. Numbers in grey
940 indicate the results of liquid COT & CER are related to the calculation of CDNC. The differences between
941 clean and polluted conditions have all passed the significant test of 95%.

942

943

944

Group (case number)	CF	CTP	COT		CWP		CER	
			liquid	ice	liquid	ice	liquid	ice
1 Clean, dry (153)	93.8 (6.1)	393.3 (117.3)	7.2 (4.6)	7.6 (9.4)	88.7 (70.6)	149.0 (146.4)	20.4 (3.0)	36.7 (6.6)
2 Polluted, dry (128)	95.6 (5.1)	475.7 (142.8)	50.2 (24.4)	43.4 (19.3)	424.6 (275.5)	793.5 (404.7)	12.6 (2.4)	30.0 (7.0)
3 Clean, wet (155)	<i>92.7 (7.0)</i> <i>p_{1,3}>0.05</i>	457.4 (191.0)	8.6 (4.7)	10.6 (12.6)	101.9 (64.5)	207.7 (254.1)	<i>19.8 (2.5)</i> <i>p_{1,3}>0.05</i>	33.2 (4.4)
4 Polluted, wet (194)	97.8 (4.4)	<i>419.7 (141.0)</i> <i>p_{3,4}>0.05</i>	36.4 (20.6)	28.4 (21.1)	295.9 (208.7)	456.4 (412.1)	<i>12.5 (2.0)</i> <i>p_{2,4}>0.1</i>	24.4 (7.5)

946

947

948

949

950

951

952

953

954

955

956

957

958

959

960

961

962

963

964

965

966

967

968

969

970

971

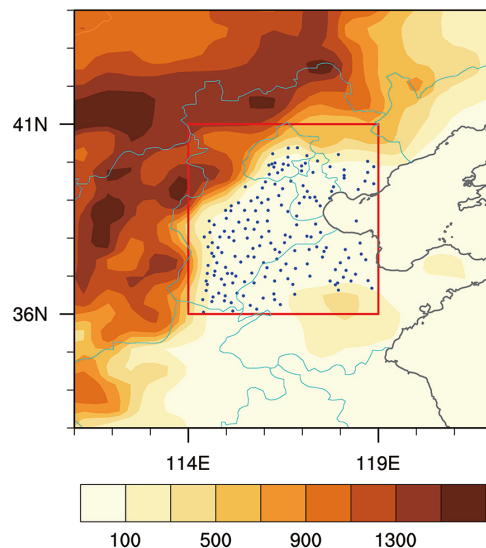
972

Table 5. The mean values of CF (units: %), CTP (units: hPa), COT (liquid and ice, units: none), CWP (liquid and ice, units: g/m³) and CER (liquid and ice, units: μm) in four groups. Numbers in the brackets stand for the standard deviations on the means. Italic numbers in grey represent that the differences are not significant, in which “P>0.05” stands for the difference has passed the significance test of 90% but did not pass the significance test of 95%, and “P>0.1” stands for the difference did not pass the significance test of 90%.

973

974 Figures

975

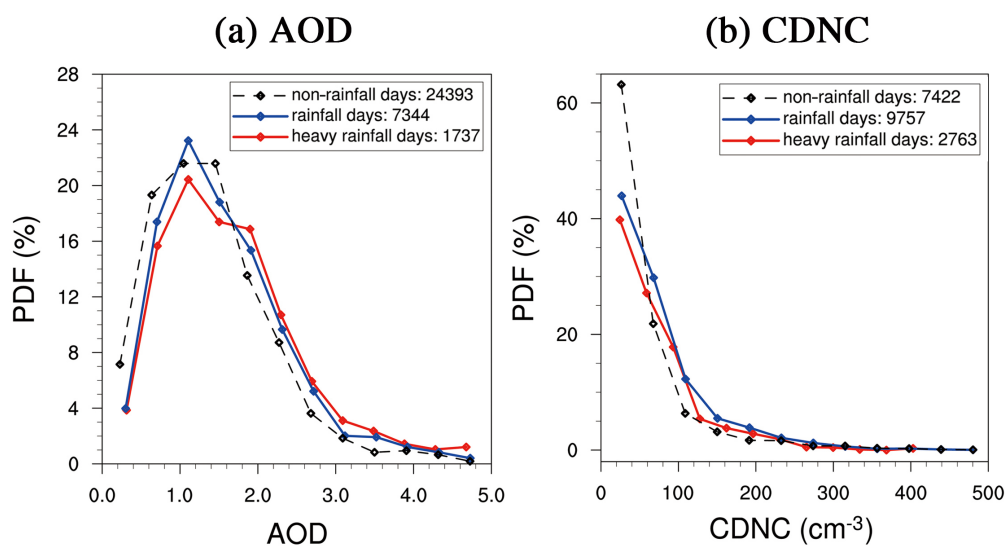


976

977 Figure 1. Selected rainfall stations (blue dots) and topography (shading, units: m) in the BTH region (red box,
978 36–41° N, 114–119° E).

979

980

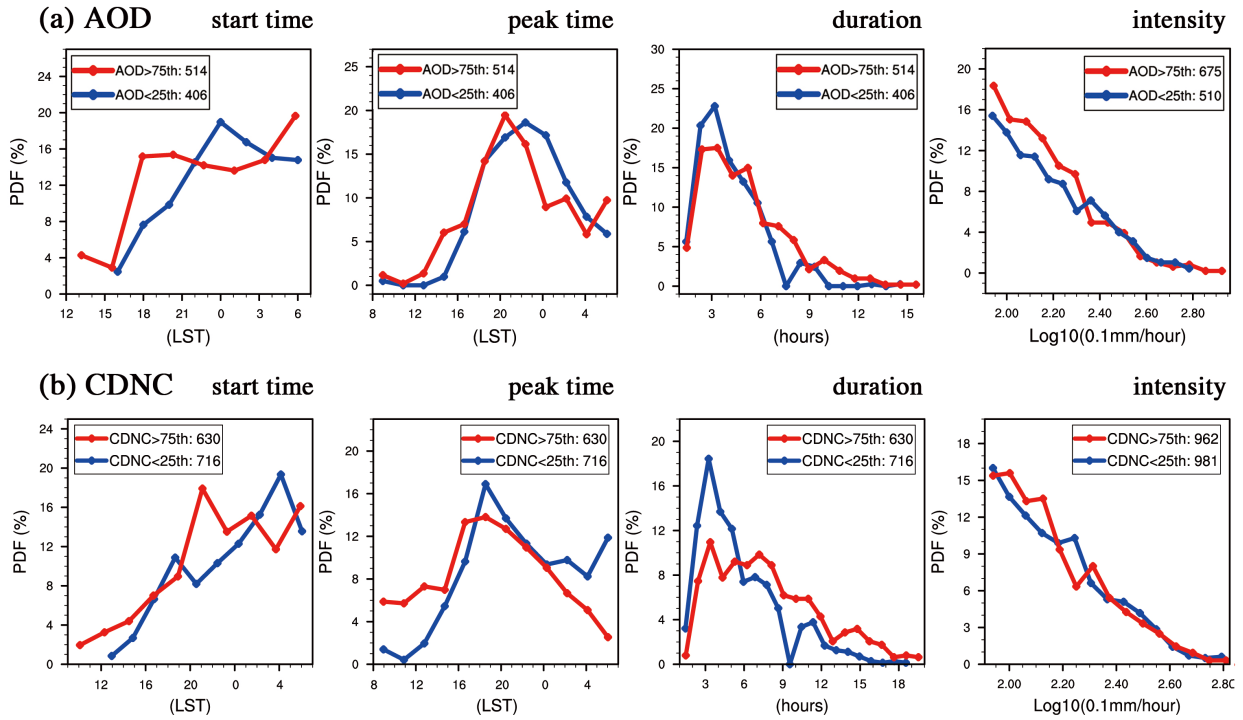


981

982 Figure 2. PDF of (a) AOD and (b) CDNC (cm⁻³) (data from MODIS) on non-rainfall days (black lines),
983 rainfall days (blue lines) and heavy rainfall days (red lines) in southwesterly during early summers from 2002
984 to 2012. Numbers in the legends denote the sample number.

985

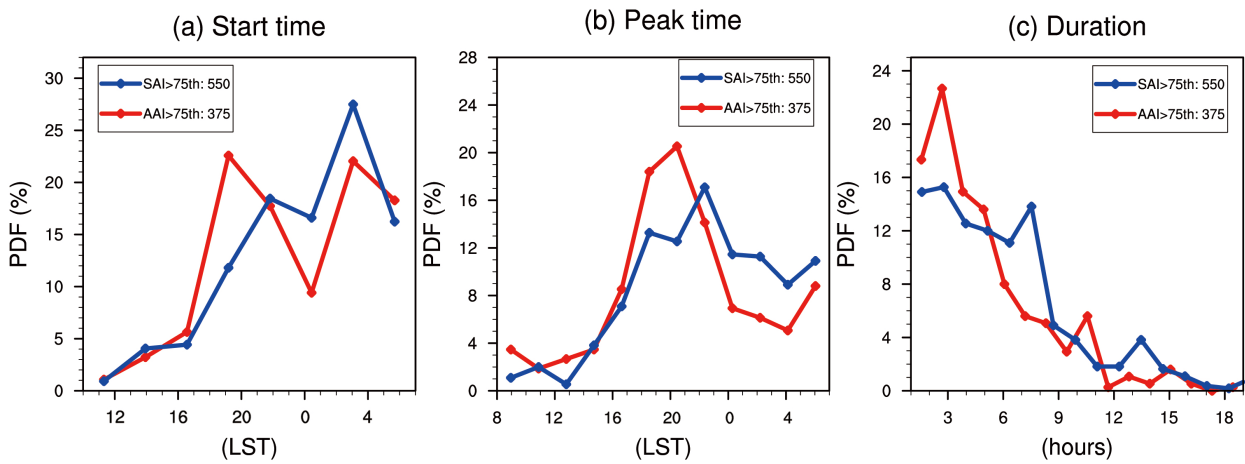
986



988

989 Figure 3. PDF of start time (units: LST), peak time (units: LST), duration (units: hours) and intensity (units:
 990 0.1mm/hour) of heavy rainfall (data from CMA) on selected clean (blue lines) and polluted (red lines)
 991 conditions, respectively using indicator of (a) AOD and (b) CDNC (cm^{-3}), during early summers from 2002 to
 992 2012.

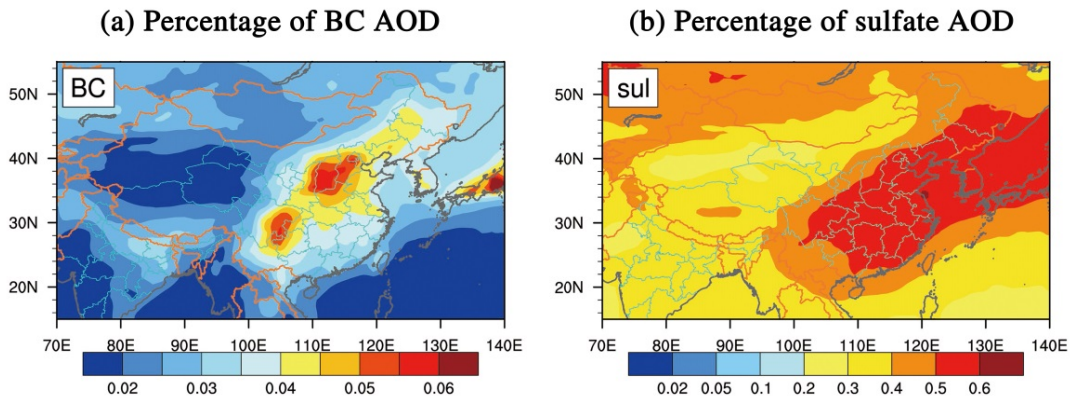
993



994

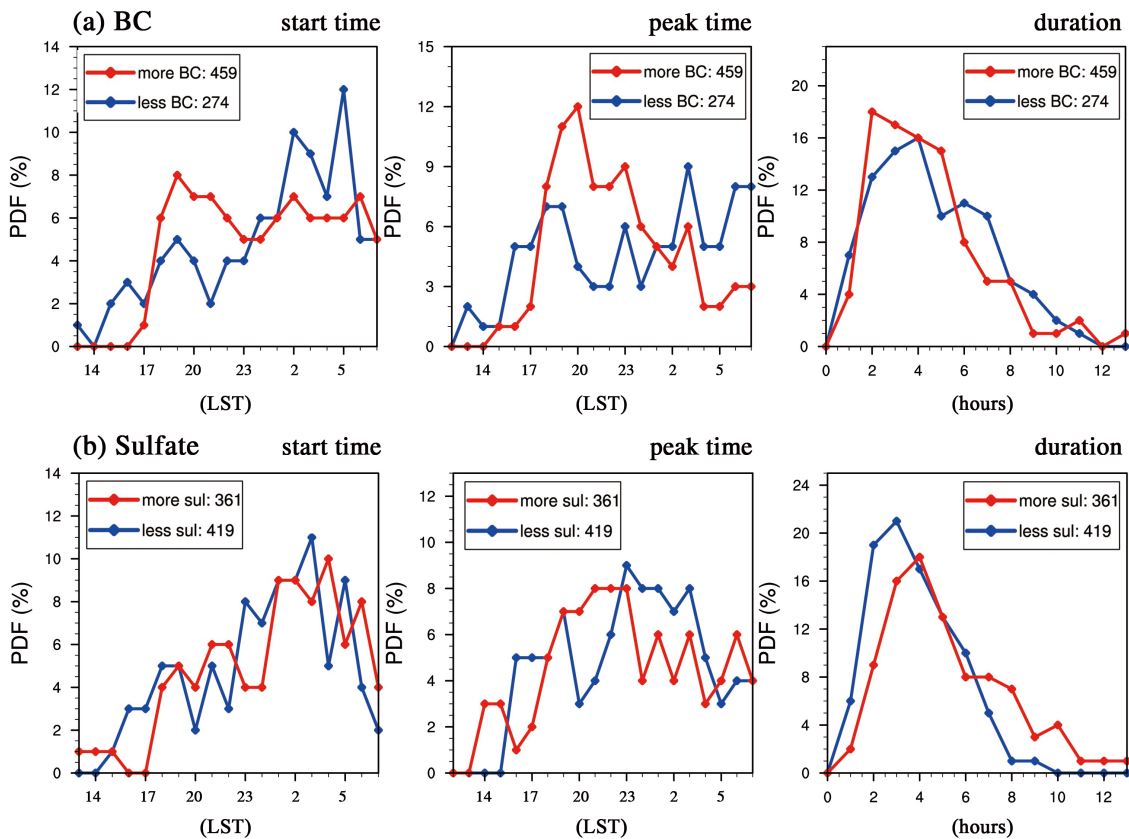
995 Figure 4. PDF of (a) start time (units: LST), (b) peak time (units: LST), and (c) duration (units: hours) of
 996 heavy rainfall on the days with SAI more than 75th percentile (blue lines, data from OMI) and days with AAI
 997 more than 75th percentile (red lines, data from OMI), during early summers from 2005 to 2012.

998



.000
.001
.002
.003
.004
.005

Figure 5. Percentages of AOD for (a) BC and (b) sulfate from MACC reanalysis data in summers (June – August) during 2002 to 2012.



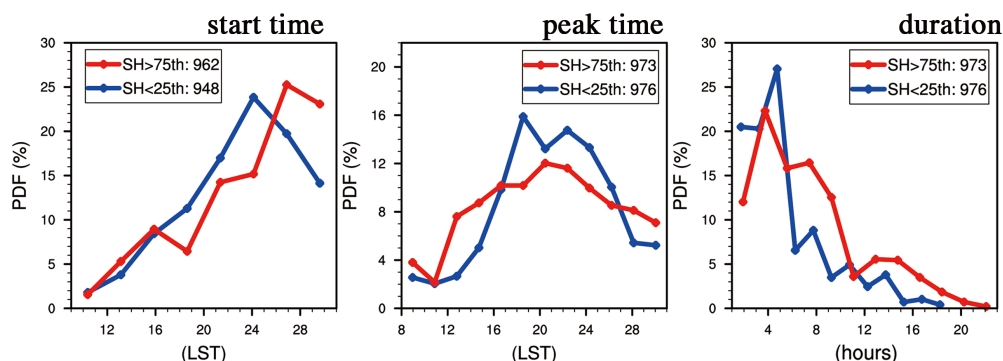
.006
.007
.008
.009
.010

Figure 6. PDF of start time (units: LST), peak time (units: LST) and duration (units: hours) of heavy rainfall on the different conditions of (a) BC and (b) sulfate. Blue/red lines stand for the condition of less/more BC or sulfate (AOD of BC or sulfate less than 25th /more than 75th percentile, data from MACC) during early summers from 2003 to 2012.

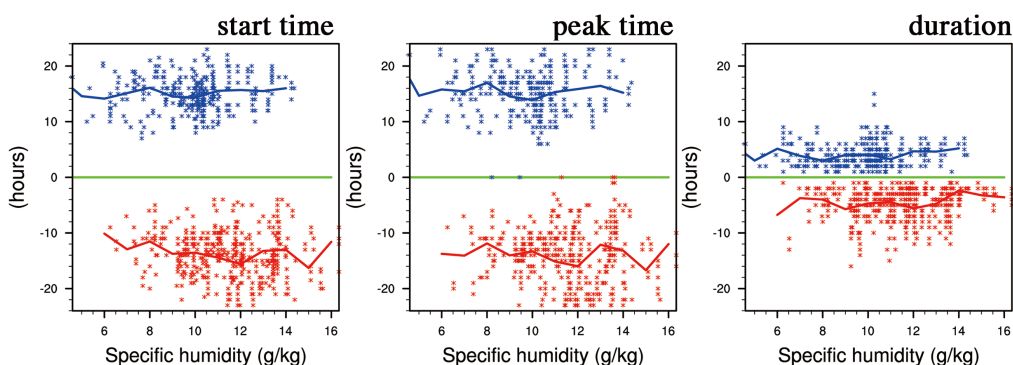
.011

.012

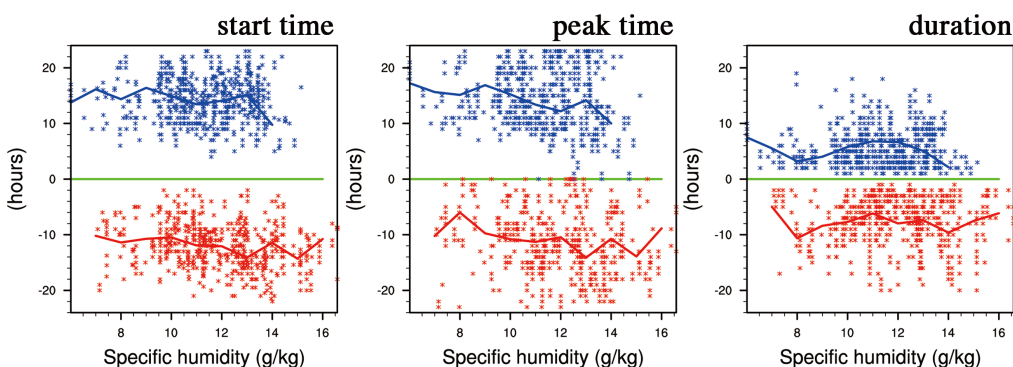
(a) PDF with more/less SH



(b) Scatter distribution using AOD



(c) Scatter distribution using CDNC



.013

.014 Figure 7. (a) PDF of start time (units: LST), peak time (units: LST), and duration (units: hours) of heavy

.015 rainfall with less moisture (blue lines, SH at 850 hPa less than 25th percentile, data form ERA-interim) and

.016 more moisture (red lines, SH at 850 hPa more than 75th percentile, data form ERA-interim). (b) and (c) are

.017 scatter distributions of SH-start time/peak time/duration for clean cases (blue points) and polluted cases (red

.018 points) respectively using AOD and CDNC. Green lines stands for the start/peak time at 8:00 LST or the

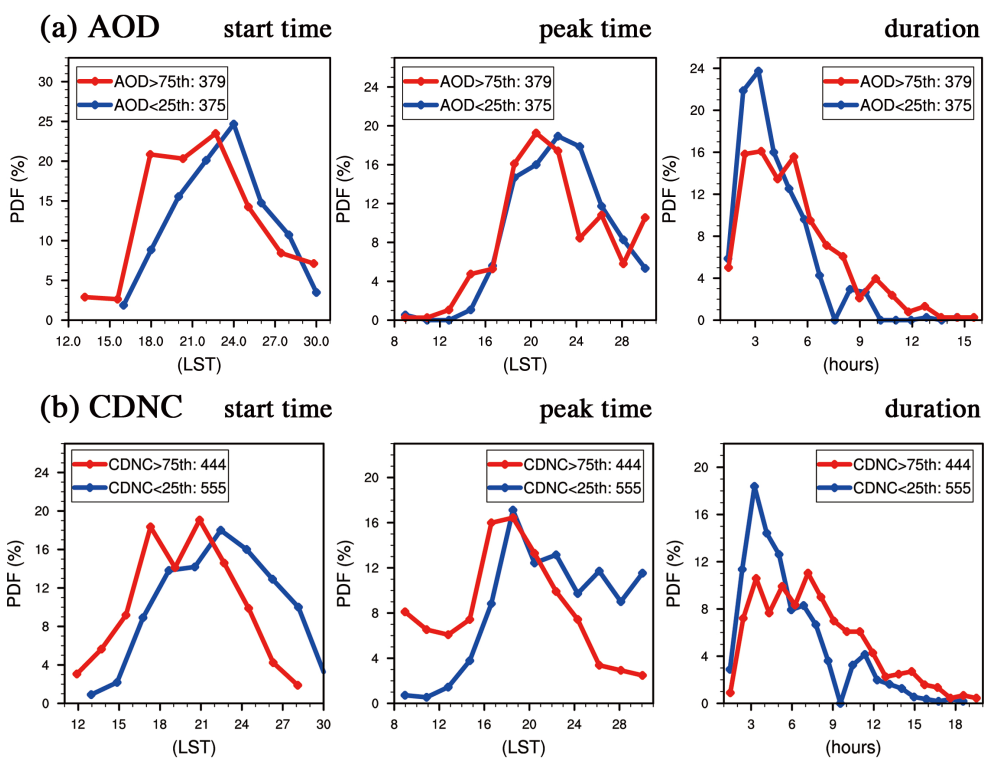
.019 duration is 0 hours. Positive (negative) values stand for the hours away from 8:00 LST or 0 hours in clean

.020 (polluted) cases. Blue (red) lines stand for the mean values of rainfall characteristics at each integer of SH in

.021 clean (polluted) cases.

.022

.023



.024

.025

.026 Figure 8. PDF of start time (units: LST), peak time (units: LST), and duration (units: hours) of heavy rainfall
.027 on selected clean (blue lines) and polluted (red lines) conditions with SH at 850 hPa (from ERA-interim) less
.028 than 75th percentile, respectively using indicator of (a) AOD and (b) CDNC (cm^{-3}), during early summers from
.029 2002 to 2012.

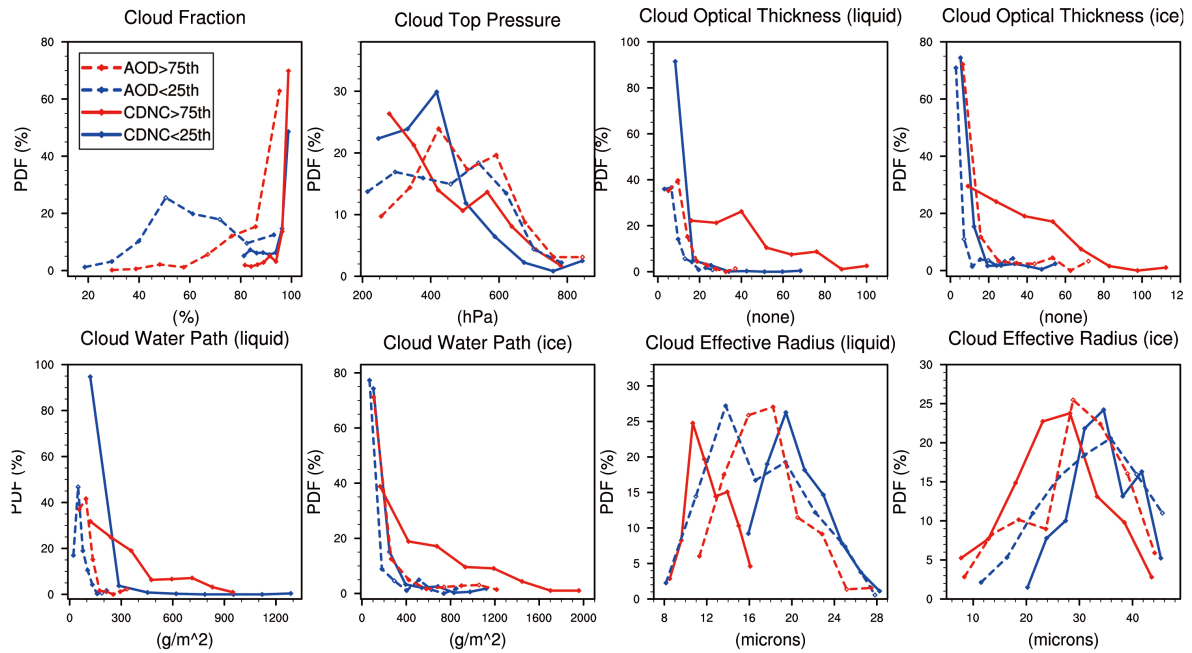
.030

.031

.032

.033

.034



.035

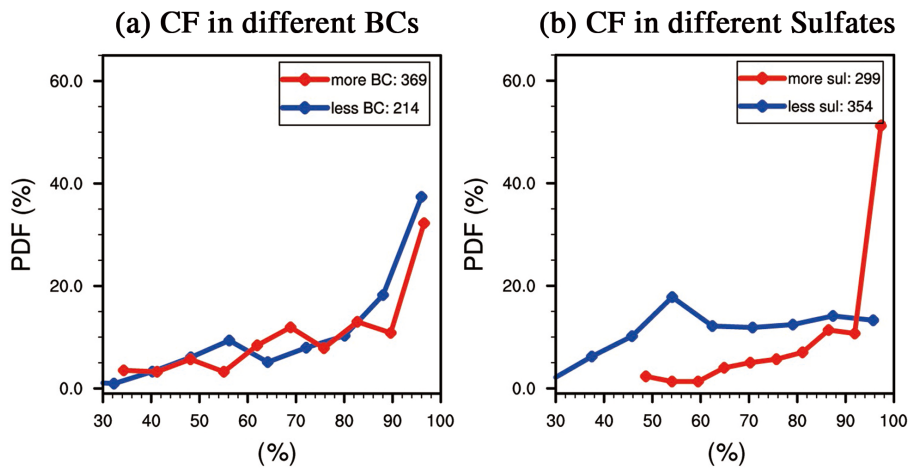
.036 Figure 9. PDF of CF (units: %), CTP (units: hPa), COT (liquid and ice, units: none), CWP (liquid and ice,
 .037 units: g/m^2) and CER (liquid and ice, units: μm) on selected clean (blue dash lines: AOD<25th percentile; blue
 .038 solid lines: CDNC<25th percentile) and polluted (red dash lines: AOD>75th percentile; red solid lines:
 .039 CDNC>75th percentile) heavy rainfall days. All cloud variables are obtained from MODIS C6 cloud product.

.040

.041

.042

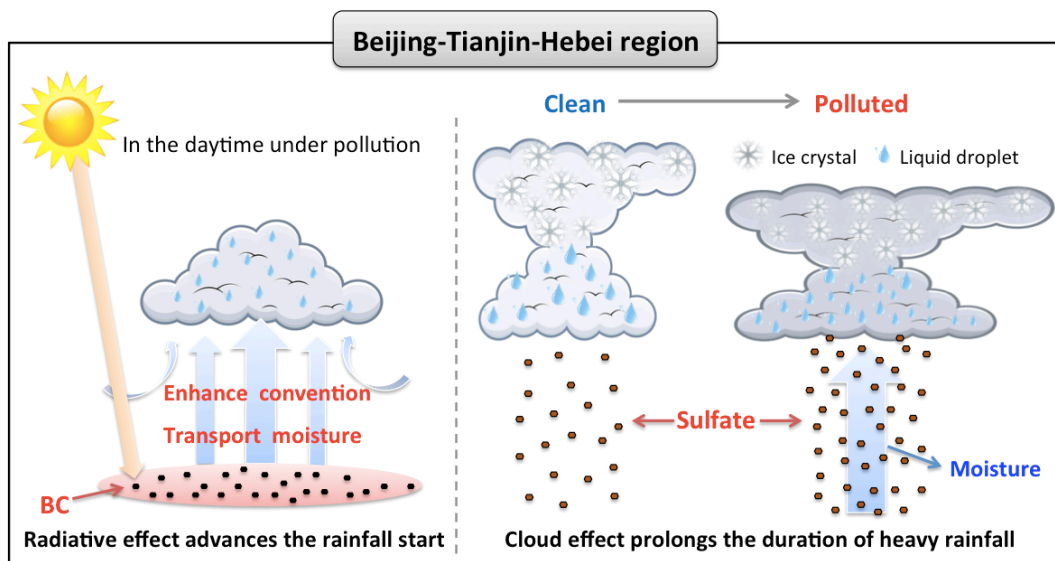
.043



.044

.045 Figure 10. PDF of CF (units: %, data from MODIS) respectively for the conditions of less BC/sulfate (blue
 .046 lines, AOD of BC/sulfate less than 25th percentile, data from MACC) and more BC/sulfate (red lines, AOD of
 .047 BC/sulfate more than 75th percentile, data from MACC) cases with heavy rainfall during 10 early summers
 .048 (2003-2012).

.049
.050
.051



.052
.053
.054
.055
.056

Figure 11. A schematic diagram for aerosol impacts on heavy rainfall over Beijing-Tianjin-Hebei region.